DOCKETED	
Docket Number:	25-OPT-02
Project Title:	Prairie Song Reliability Project
TN #:	269416
Document Title:	Jacqueline Ayer Comments - Letter from Save Our Rural Town
Description:	N/A
Filer:	System
Organization:	Jacqueline Ayer
Submitter Role:	Public
Submission Date:	4/6/2026 1:36:39 PM
Docketed Date:	4/6/2026

Comment Received From: Jacqueline Ayer
Submitted On: 4/6/2026
Docket Number: 25-OPT-02

Comment letter from Save Our Rural Town

Comment letter from Save Our Rural Town

Additional submitted attachment is included below.

SAVE OUR RURAL TOWN

April 6, 2026

Lisa Worrall
Project Manager
California Energy Commission
715 P Street, MS-40
Sacramento, CA 95814
Submittal of a 20 page letter and 2 attachments

Subject: Supplemental Comments by Save Our Rural Town (SORT) pertaining to the "Data Request Response 6" Provided for a Proposed Battery Energy Storage Project in Acton, CA.

Reference: California Energy Commission Docket Number 25-OPT-02.

Dear Ms. Worrall;

Save Our Rural Town (SORT) respectfully offers the following supplemental comments in response to the "Data Request Response 6" filed by "Prairie Song Reliability Project LLC" (developer) in response to information requests issued by the California Energy Commission (Commission) pursuant to the referenced licensing Application. The developer seeks to construct a 9,200 MWh Battery Energy Storage System (BESS) that will stretch more than a mile in length within the rural community of Acton in unincorporated Los Angeles County.

SORT has carefully reviewed the developer's responses to the Commission's information request, and we have a number of concerns regarding the material provided therein. These concerns range from relatively minor deficiencies (such as the fact that the developer once again submitted AERMOD output files in a portrait format which makes them difficult to read and did not provide concentration plots of toxic compounds so that exposure impacts can be properly visualized) to very serious concerns regarding conclusions derived from modeled results and the derivation of emission factors which form the basis of the modeled results. These more serious concerns are set forth below; they are arranged in a format that parallels the format of the developer's data request responses.

SORT DISPUTES RESPONSES TO INFORMATION REQUEST #2.

In the response to "Request for Information #2", the developer states that the dataset used in the AERMOD analysis included the "evaluation of the wind rose derived from the Palmdale Airport meteorological data station and the wind rose of the weather station in Acton". However, the developer does not provide the Acton wind rose, and the AERMOD analysis appears to be based entirely on Palmdale airport wind rose data; accordingly, the AERMOD results do not "evaluate" or otherwise account for Acton weather conditions. Additionally, the omission of the Acton weather station wind rose is a substantial deficiency: if it had been included, the public and decisionmakers could assess whether the Palmdale meteorological data (and by extension, the AERMOD results) properly and accurately represent actual conditions at or near the project site. SORT urges the developer to provide the Acton Wind Rose data.

Additionally, the response to "Request for Information #2" alleges that the maximally exposed individual receptor (MEIR) is located 394942.29 meters east, 3816484.92 meters north (in UTM coordinates); SORT has determined that this location coincides with the center of the Benitez's home on Assessor Parcel 3056-019-034. According to the response to "Request for Information #7", the 1-hour χ/Q value at this location is 872.1 in $(\mu g/m^3)/(g/s)$. Reconciling this with the developer's alleged HF release rate of 0.17 g/s yields a concentration at this location of 148.3 $\mu g/m^3$ which is well below the 240 $\mu g/m^3$ significance threshold established for HF. However, the response to "Request for Information #7" also alleges that the location identified as 394894.43 meters east, 3816484.27 meters north has a χ/Q value of 1616.1 $(\mu g/m^3)/(g/s)$ and the location identified as 394918.36 meters east, 3816484.59 meters north has a χ/Q value of 1428.7 $(\mu g/m^3)/(g/s)$. These χ/Q values correspond to HF concentrations of 274.7 $\mu g/m^3$ and 242.9 $\mu g/m^3$, respectively; therefore, both locations exceed the established 240 $\mu g/m^3$ significance threshold.

Figure 1 provides a plot of these exceedances: one location is just west of the Benitez's walkway leading to their front door; the other is just west of the Benitez's barn and southeast of their horse corral. Both of these points are locations where a receptor is likely to be found. Accordingly, the AERMOD results show that, if the developer's assumed HF emission rate is accurate (a point which SORT *does not* concede) and the developer's wind data represents conditions in Acton (another point which SORT *does not* concede), the project will clearly result in HF concentrations that exceed the established significance threshold at likely receptor locations. Therefore, the project poses a significant public safety risk.

Moreover, these results demonstrate that the actual location of the MEIR hinges entirely on the location of the BESS that is modeled. For example, and as indicated in Figure 1, the 1616.1 χ/Q value is 227 feet from the modeled BESS location, and it lands 325 feet

Figure 1: Plot of χ/Q Values Determined by the Developer's AERMOD Analysis.

due east of the Bavaro home; therefore, shifting the location of the modeled BESS to the west by 325 feet will place the 1616.1 χ/Q (and the HF concentration of 274.7 μg/m3) squarely on the Bavaro home. Similarly, shifting the modeled BESS further south and west will place the 1616.1 χ/Q value and 274.7 μg/m3 HF concentration on the Quevedo home and even the Ramirez home. These facts demonstrate that there are numerous potential locations where a BESS fire will result in concentrations that exceed the 240 μg/m3 significance threshold because the BESS yard is more than 3,500 feet long and 600 feet wide. These facts also suggest that the modeled BESS location was carefully chosen to ensure that the χ/Q value at the home that was selected as the MEIR would results in less than significant constituent concentrations that are below significance thresholds. Such a contrivance would be very disappointing.

According to the developer's response to "Request for Information #2", the BESS location that was modeled (394880.53 meters east, 3816417.74 meters north in UTM coordinates) was chosen because the developer believed that it is "the shortest downwind distance to nearby sensitive receptors under prevailing wind conditions"; this receptor location (the Benitez home) is described as being "approximately 89 meters (approximately 292 feet) from the modeled BESS container". However, the developer's most recent site plan[1] indicates that the Benitez's home is actually closer than 292 feet from the nearest BESS (see Figure 2). In fact, the site plan shows that numerous residences are closer than 292 feet to a BESS location, including:

[1] The updated site plan was provided in response to Data Request 2.

- The Quevedo property is 100 feet from the nearest BESS; the house is 150 feet from it. [Assessor Parce Number 3056-019-035].
- The Ramirez property is 100 feet from the nearest BESS; the house is 160 feet from it. [Assessor Parce Number 3056-019-036].
- The Bavaro property is 100 feet from the nearest BESS; the house is 165 feet from it. [Assessor Parce Number 3056-019-004].
- The Cervantes property is 130 feet from the nearest BESS; the house is 225 feet from it. [Assessor Parce Number 3056-022-036].
- The Devore property is 80 feet from the nearest BESS; the house is 238 feet from it. [Assessor Parce Number 3056-019-010]
- The Lenarth property is 160 feet from the nearest BESS; the house is 205 feet from it. [Assessor Parce Number 3056-019-039].
- The second Lenarth property is 160 feet from the nearest BESS; the house is 210 feet from it. [Assessor Parce Number 3056-019-045].

Figure 2. Site Plan Excerpt Showing Proximity of BESS to the Benitez Home.

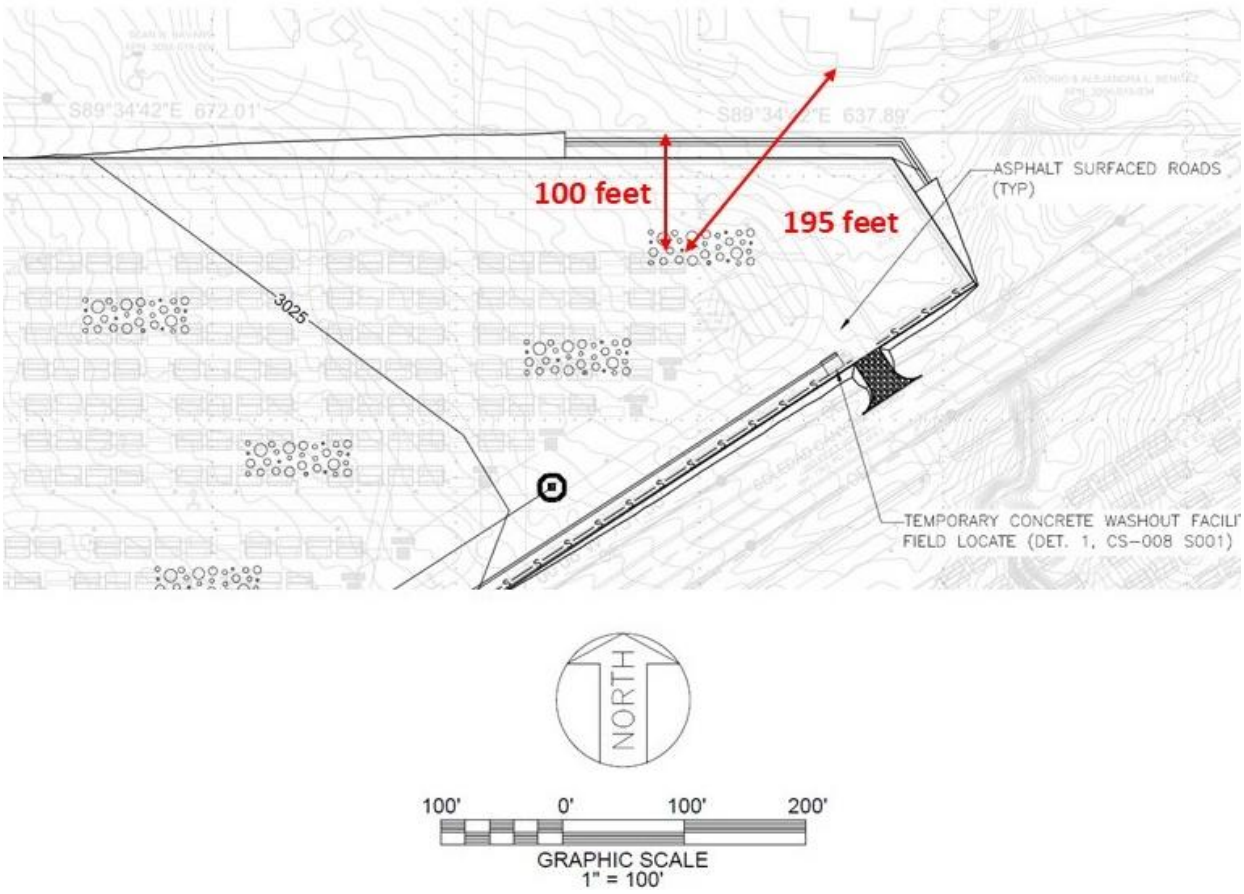

It appears that these properties were not considered in the developer's dispersion model because they are on the west end of the project and thus not aligned with the modeled wind pattern (which is toward northeast and is based on Palmdale meteorological data). The problem is, the wind in Acton frequently blows *from* the northeast particularly in the fall and winter during "fireweather" conditions (which is why Southern California Edison is constantly shutting off power in Acton during these seasons). The developer confirms on page 16 that the predominant wind pattern in Acton is from the northeast. If actual wind patterns in Acton had been taken into consideration by the AERMOD analysis, the properties identified above would been evaluated as potential MEIR locations. SORT is concerned that the developer's AERMOD results do not reflect actual exposure conditions that will occur whenever a BESS device ignites. Moreover, SORT disputes the developer's assumption that MEIR locations are limited to just dwelling structures. Given that the properties surrounding the BESS project are used for agricultural purposes and that residents are frequently found outside their homes, all areas of work outside their residences. Accordingly, all areas the parcels that surround the project site should be considered potential MEIR locations, not just homes.

SORT DISPUTES THE RESPONSE TO "REQUEST FOR INFORMATION #5".
In response to "Request for Information #5", the developer provides information pertaining to the derivation of emission that were used as inputs to the AERMOD program. SORT has carefully analyzed this information, and found that it is based on a technical study which is fatally flawed and substantially understates HF emissions.

Specifically, the developer's HF emission factor is based on a study conducted by Liu et al. (the Liu Study[2]) that analyzed "pouch" type battery cells[3]. Notably, the PowerTitan 2 BESS proposed by the developer utilizes cylindrical battery cells, not pouch cells[4]. Nonetheless, the developer contends that the Liu Study is the appropriate foundation for estimating HF emissions from a PowerTitan 2 BESS because it analyzed "large format" battery cells that are representative of "containerized BESS fires" rather than small battery cells such as those analyzed by Larsson et al. (the Larsson Study). Notably, the Liu Study relied on an analytical methodology involving a Fourier Transform Infrared (FTIR) Analyzer which, under the right circumstances, can be useful for measuring HF (as SORT has previously pointed out[5]). However, the sampling system adopted by the Liu Study introduced substantial bias into the FTIR's HF measurements and as a result, the Liu Study substantially underreports actual HF emissions. There are several reasons for this:

[2] SORT cannot provide a copy of the Liu Study because of copyright laws, but it can be purchased for $36.
[3] The Liu Studied analyzed a 243Ah battery described as "two *pouch cells* connected in parallel".
[4] See for example page 10 of the developer's response to Data Request #5.
[5] See page 17 of SORT's Scoping Comments dated March 4, 2026.

- According to page 2, before the sample gas was introduced into the FTIR optical chamber, it was "pretreated" and "dried". This is typically done because water is highly absorbing in the infrared band; thus, water vapor in the sample gas interferes substantially with FTIR measurements[6]. This is particularly true when measuring constituent concentrations in a combustion environment because the combustion process generates substantial quantities of water vapor. Moreover, HF is highly soluble in water; thus, when the sample stream was "dried" before it entered the FTIR optical chamber, most of the HF in the sample stream was removed with the water vapor. *This caused a substantial low bias in the measured HF results.*

- According to Figure 2, sample gas was not extracted near the burn zone; rather, it was extracted far downstream of where the exhaust gas was first collected by a large vent housing (presumably metal) and then traveled through an exhaust duct (also presumably metal). Because HF is highly reactive, it adsorbed onto the metal surfaces and reacted which removed it from the sample stream. Therefore, this sampling arrangement caused *substantial HF attrition and biased the results.*

- Standard FTIR equipment (such as KBr optics) reacts with HF even at very low concentrations; therefore, special FTIR optics are required when monitoring for HF. The Liu Study does not provide any information regarding how the FTIR was setup; however, it is doubtful that special optics were used because if they were, the authors would have certainly mentioned it. Therefore, it is likely that standard FTIR optics were used, in which case *more HF was probably removed via reaction with FTIR optical equipment.*

All of the circumstances present in the Liu Study (sample gas "drying" which removed much of the HF, the long distance between the burn zone and the sampling point which created significant HF adsorption losses, and probably standard FTIR optics) result in HF measurements that are *heavily biased low* and thus substantially *understated.* Accordingly, the Liu Study ***is not*** an appropriate foundation for an HF emission factor because it ***does not*** accurately measure HF emissions.

SORT is not alone in pointing out that the HF results reported by the Liu Study are heavily biased; in fact, the authors themselves admit to this problem because page 8 states that HF was lost "because it is highly soluble in water and its reactivity with alkaline products". In short, the Liu Study is *admittedly unreliable* for assessing HF emissions from battery fires and *must not be used* to estimate HF emissions from *any* battery fire. It certainly cannot be relied upon to estimate HF emissions from the PowerTitan 2 BESS that is proposed by the developer.

[6] SORT's Director, Jacqueline Ayer, has extensive experience in extractive FTIR sampling methodologies and has used FTIRs for monitoring toxic constituent concentrations in paint booth exhaust systems.

A paper published by Yan et al. from the University of California at Los Angeles in August, 2025 (the UCLA Study) explains just how difficult it is to obtain accurate HF emission data from the combustion environment created by battery fires. This study (provided in Attachment 1) explains on page 1 that "in situ" sampling is difficult, and that using FTIR instrumentation has limitations. It also explains that placing the analytical instruments far from the burn zone results in reaction and adsorption losses *particularly when highly reactive constituents (like HF) are present*; it also results in sampling dispersion and measurement latency. All of these circumstances are found in the Liu Study (as explained above); therefore, the Liu Study is unreliable. On page 3, the authors describe how the UCLA Study measured in situ HF concentrations using laser infrared absorption spectroscopy and how they were able to overcome water vapor interference in the selected IR band using Boltzmann intensity distribution. This allowed them to measure HF concentrations directly in the burn zone without having to first "dry" the sample gas to remove moisture before analyzing it. Because the UCLA Study measured HF concentrations directly in the burn zone without duct attrition or "drying" losses, it does not suffer from the heavy bias that plagues the Liu Study.

Notably, the UCLA Study found that the highest HF emissions occur during the onset of emergency venting[7], and Table 1 reports that HF accounts for up to 9% of the total battery weight loss during venting. This is very troubling, because it means that:

- Highest HF emission rates occur at the very beginning of a BESS deflagration event;
- Highest HF exposure risk is likely to occur before emergency responders arrive and evacuation or "shelter in place" orders are issued.
- HF can account for nearly 10% of the total venting weight loss.

Together, these facts indicate that a BESS fire at the proposed project would likely release significant quantities of HF and expose Acton residents to dangerous HF levels without warning.

SORT offers the UCLA Study as further proof of why the Liu Study should not serve as the foundation for any HF toxic risk assessment. And, though the sampling and analysis methodology adopted by the UCLA Study provides a much more reliable quantification of HF emissions from lithium battery fires than the Liu Study, it does not provide much information regarding the batteries that were studied other than that they were "Sanyo NCR 18650 GA" cylinder cells. Given this, SORT does not necessarily suggest that the UCLA Study should be used as the basis for estimating HF emissions from a PowerTitan 2 BESS fire; however, the UCLA Study seems more reliable than the Liu Study.

[7] This is perhaps one reason why HF sampling at active BESS fires (which are not initiated until hours or even days after a BESS ignition) do not show high concentrations.

ADDITIONAL CONCERNS REGARDING THE DEVELOPER'S RESPONSE TO "REQUEST FOR INFORMATION #5".

In the response to "Request for Information #5" the developer describes how the HF emission factor was derived for input to the AERMOD model. Putting aside the fact that HF emission factor is founded on the Liu Study which substantially underreports HF concentrations, there are other problems with the derivation as well. For instance, the 5.45 gram HF mass emission value that the developer used is not the peak value reported in the Liu Study; rather it is an average value. This is neither conservative nor reasonable (particularly since the authors of the Liu Study openly admit that the HF concentrations are too low). At the very least, the developer should have used the peak HF mass emission value from the Liu Study (8.1 grams) rather than the average value of 5.45 grams.

Additionally, the developer chose to calculate the HF emission factor based on battery weight rather than energy capacity or some other unit. This approach is insupportable because cylindrical batteries (such as those used in the PowerTitan 2[8]) tend to be much heavier per Wh than the pouch battery cells tested in the Liu Study[9]. More importantly, the Liu Study did not reveal the mass of the pouch battery cells that were tested; accordingly, the Liu Study does not even provide the data that is necessary to develop a "weight based" HF emission factor. To overcome this deficiency, the developer used the mass of the cylinder-based PowerTitan 2 battery cells to "estimate" a hypothetical mass for the pouch batteries analyzed in the Liu Study; this hypothetical mass is 4.31 kg. However, using the mass of a cylinder battery to determine an HF mass emission factor for a pouch battery will provide erroneously low and arguably baseless results[10].

Next, the developer reconciles this hypothetical 4.31 kg value with the average 5.45 gram mass emission value from the Liu Study to estimate a theoretical weight-based HF emission factor as follows:

Eq. 1
$$5.45\ g\ \text{HF} \times \left(\frac{1000\ mg\ \text{HF}}{g\ HF}\right) \times \frac{1}{4.31\ kg\ \text{battery}} = 1264.5\ mg\ \text{HF/kg of battery weight}$$

(For reasons that are not clear, the developer reports on page 7 that the resultant value is 1,236.7 mg/kg; this is incorrect. The correct value is 1264.5 mg/kg)

---

[8] See for example page 10 of the developer's response to Data Request #5.

[9] Cylinder batteries have more casing material than pouch batteries, See for example https://battlebornbatteries.com/pouch-vs-prismatic-vs-cylindrical-lithium-battery-cells/#

[10] Given that pouch batteries are lighter than cylinder batteries, the use of a cylinder battery mass to estimate a pouch battery emission factor will result in a lower mass-based emission factor. This is because the denominator (which represents the mass value) is large if it is based on a cylinder battery mass value; this in turn results in a smaller HF emission factor. On the other hand, if the denominator is based on a pouch battery mass (which is a smaller number) then the HF emission factor will be larger.

Next, the developer applies a 50% correction (which, as discussed in more detail below, is also unsupportable) to derive a 631.86 mg/kg emission factor and then converts the whole thing into English units to claim that the PowerTitan 2 BESS will only emit 0.00063 pounds of HF per pound of battery. This HF emission factor is "shaky" at best because it is founded on the heavily flawed Liu Study, it is based on a hypothetical (and erroneous) mass value, and it is further biased by the application of an unsubstantiated 50% correction factor. Nothing about the developer's HF emission calculation is reasonable, conservative, or appropriate for a toxic risk exposure assessment.

Finally, SORT notes that the developer's claim that HF emissions should be expressed as a function of battery weight is not supported by facts or evidence[11]. Moreover, substantial evidence demonstrates that this claim is erroneous. For example, the UCLA study explains that a principal source of HF emissions from a BESS fire is the electrolyte, and that most of it is emitted at the beginning during emergency venting "because the primary source of HF is electrolyte decomposition, *which occurs at relatively low temperatures*" (emphasis added)[12]. Therefore, HF emissions are largely driven by the amount of electrolyte in the BESS, not the weight. Furthermore, pouch cells and cylinder cells have substantially different configurations which lead to differences in mass densities, energy densities, electrolyte character, and other factors[13] all of which affect HF emissions. Accordingly, the premise that an HF emission factor should be based solely on BESS weight regardless of battery type (pouch vs cylinder) or electrolyte characteristics (total amount or amount of $LiPF_6$) lacks foundation.

SORT DISPUTES THE RESPONSE TO "REQUEST FOR INFORMATION #6".
In the response to "Request for Information 6", the developer devotes several pages to arguing why the 38.86 pound HF emission value that was input to the AERMOD program is conservatively appropriate. In the paragraphs below, SORT disputes all of the developer's contentions. For simplicity, these paragraphs are arranged sequentially to mirror the developer's arguments which are indicated in italics.

Page 8: The developer argues that the Larsson Study is not relevant because it only analyzed small format batteries. This argument ignores the fact that the electrolyte is the principal source of HF emissions; therefore, if small and large format batteries use similar electrolyte chemistries, some parallels can reasonably be drawn as long as the differences between pouch and cylinder cells is taken into account.

---

[11] The Ramboll study provides no justification for establishing an HF emission factor based on battery weight; instead Footnote 109 just states that HF emissions are expressed in terms of battery mass.
[12] Yan, Y., Jaeger, N.S.B., Spearrin, R.M., "*Hydrogen fluoride emissions from lithium-ion batteries during induced thermal runaway via in situ laser spectroscopy*". Department of Mechanical and Aerospace Engineering, University of California, Los Angeles. At 6.
[13] See https://battlebornbatteries.com/pouch-vs-prismatic-vs-cylindrical-lithium-battery-cells/#

Page 8: The developer argues that the Larsson Study does not report HF emissions in units of milligrams per kg of battery weight and instead reports HF emissions in units of milligrams per gram of mass lost. This argument is odd, given that the Liu Study upon which the developer's HF emission factor is based also recorded mass loss data and not total mass. In fact, the Liu Study did not even report the weight of the battery cells that were tested. Moreover, the developer does not explain or justify why HF emissions should be reported as a function of battery weight, especially since HF emissions appear to be more related to battery type and electrolyte characteristics.

Page 8: The developer argues that the purpose of the Larsson Study was to characterize HF estimates as hypothetical extrapolations to illustrate potential hazards and not for consequence modeling. This argument is odd, given that the purpose of the Liu Study was also to characterize HF estimates and thereby illustrate potential hazards and not for consequence modeling. In fact, the Liu Study was performed specifically to illustrate potential hazards for the purpose of developing "active interventions to minimize the damage"; it also hypothetically extrapolated HF measurements to predict resultant concentrations in a 50 m^3 room to assess potential hazards. Like the Larsson Study, the Liu Study characterizes HF estimates as hypothetical extrapolations to illustrate hazards and not for consequence modeling.

Pages 8-9: The developer argues that the modeling objective was to minimize reliance on "hypothetical extrapolation" and instead use emission factors reported on a battery mass basis from tests that closely align with flaming thermal runaway conditions relevant to containerized BESS fires. However, the developer's HF emission factor is intrinsically a "hypothetical extrapolation" because it is based on an average of flawed HF results from the Liu Study and it hypothetically estimates the mass of the battery used in the Liu Study. Therefore, the developer's HF emission factor is not closely aligned with "flaming thermal runaway conditions relevant to containerized BESS fires".

Page 9: The developer argues that the test scale, combustion condition, and normalization method adopted in the Larsson Study are not suited for "representing a full containerized LFP BESS fire for off-site plume modeling". Here, the developer argues that the results from the Larsson Study are not "suitable" for use in a health risk exposure assessment. However, and regardless of the applicability of the Larsson Study, the developer does not appear to grasp here is that the Liu Study is singularly ***not*** "suitable" for use in a health risk exposure assessment for the reasons set forth above.

Page 9: The developer contends that the 631.86 mg/kg of battery HF emission factor is conservative and ensures "a health-protective assessment" because it is based on the peer reviewed Liu Study. Because the Liu Study substantially underreports HF emissions, the developer's 631.86 mg/kg emission factor is not conservative; to the

contrary, it is intrinsically low and is rendered even more inaccurate with the addition of an uncorroborated 50% correction factor. Accordingly, the 631.86 mg/kg HF emission factor is ***not*** representative of the Project's BESS fire scenario, it is ***not*** conservative, and it certainly does ***not*** ensure "a health-protective assessment".

Page 9: The developer argues that the Liu Study conducted controlled burn tests and reported emission yields "on a mass-normalized basis (mg/kg of battery)". This statement is incorrect because the Liu Study does not report emission yields based on mg/kg of battery; to the contrary, the Liu Study focused only on battery mass loss, not battery mass. In fact, and as explained above, the Liu Study does not even report battery weights (which is why the developer had to hypothetically estimate the weight of the battery tested by Liu et al. so that it could be force-fitted into the developer's mass emission factor calculation). To be clear, Section 3.4 of the Liu Study unequivocally establishes that "mass loss" was recorded, not battery mass.

Page 9: The developer argues that, because the Liu Study considered an LFP battery chemistry, the Liu Study results are applicable to the project, they reflect the failure mode of a containerized BESS, and the modeling captures conditions of a fully developed battery fire. What this argument fails to consider is that the Liu Study substantially understates HF emissions; therefore, it is not applicable to the project and it does not reflect the potential failure mode of a containerized BESS. Therefore, the modeling ***does not*** capture conditions of a fully developed battery fire.

Page 10: The developer contends that the Larsson Study found that pouch batteries release higher amounts of HF likely because cylinder batteries build up pressure before rupture, leading to a shorter duration of combustion. This statement is incorrect. The Larsson Study *does not* posit that pressure buildup is the *likely* cause of lower HF emissions from cylinder batteries. To the contrary, the Larsson Study attributes the difference to differing amounts of electrolyte and materials; the Larsson Study only offers the pressure theory as a possible explanation, but then states results "are difficult to explain" (bottom of page 2).

Page 10: The developer contends that a 50% correction factor based on the 2017 Larsson Study is applicable to account for differences in cell format. This argument fails for several reasons. First, the 2017 Larsson Study analyzes only small format batteries; thus, using it to develop an emission factor correction contradicts the developer's position that small format battery studies are irrelevant because they do not represent full scale burn conditions. The developer cannot have it both ways: if small format battery results are useless for calculating an emission factor for a full scale BESS fire, then they are also useless for deriving emission factor corrections for a full scale BESS fire. This inconsistency alone invalidates the developer's 50% "correction factor".

Second, the 2017 Larsson Study reports that the FTIR measurement system underestimated HF levels values for the batteries which had the lowest HF emissions because "HF might not have been collected in the measurements and the effect of this error is largest for the batteries that give the lowest values [i.e. cylindrical batteries]. Thus, the reported values might underestimate the released gas emissions" (see page 10). Here, the authors explain that HF measurements of cylindrical batteries are biased low (and thus underreported) because of limitations in the sampling methodology. Because the FTIR's HF emission results reported for cylindrical batteries have a low bias, they should not be used to derive a "correction" for the developer's HF emission factor. For convenience, SORT has included the 2017 Larsson Study in Attachment 2.

Third, Table 3 in the 2017 Larsson Study shows that the FTIR measurement results are persistently and significantly underpredictive (typically by more than 50%) compared to impinger results. Thus, the FTIR measurement results may not be sufficiently reliable for the purpose of deriving a correction for the developer's HF emission factor.

Fourth, Table 7 in the 2017 Larsson study shows that 34 pouch battery tests were conducted; these included multiple replicate HF analyses using both FTIR and impinger methodologies. Yet, very few cylinder batteries were tested. In fact, only one type of cylinder battery was tested once at a single state of charge and a second type of cylinder battery was tested only once at two different states of charge; no replicate cylinder battery tests were conducted and no impinger cylinder battery tests were conducted. SORT contends that there is not sufficient data pertaining to cylinder batteries to draw substantive conclusions regarding how cylinder cell emissions compare to pouch cell emissions. Moreover, because no impinger results were collected for any cylinder battery tests, and because the authors admit that FTIR measurements of "the batteries that give the lowest values" (i.e. the cylinder batteries) are biased low, the cylinder test data collected in the 2017 Larsson Study is not sufficiently robust to use for calculating a correction to an HF emission factor. Accordingly, the developer's 50% correction factor lacks substance and is not supported by reliable evidence.

Page 10: The 2017 Larsson Study reports that LFP pouch cells at full charge produced 150–200 mg HF/Wh and cylindrical LFP cells produced roughly 12–52 mg of HF per Wh. This statement is factually incorrect. Table 3 of the 2017 Larsson Study shows that fully charged pouch cells produced 53.9-191 mg of HF per Wh, not 150-200 mg/Wh. Furthermore, Table 7 shows that multiple replicate tests were run for each of the two types of pouch batteries that were tested ("Type B" and "Type C") at several different charge states, but very few cylinder batteries were tested ("Type D" and "Type E"). The results from each test series conducted for each battery type are reported in Table 2 as a range of values. Specifically, Table 2 shows that emissions from pouch batteries ranged from 43 to 198 mg HF per Wh and emissions from cylinder batteries ranged from 12-52

mg HF per Wh. This shows that, in at least one instance, a pouch battery *actually resulted in less HF emissions per Wh* than at least one cylinder battery! This is another reason why the developer's 50% correction factor is not credible.

Page 10: Regarding the 2017 Larsson Study, the developer states "After converting to a mass basis, the cylindrical cells' HF emissions were approximately half (or even less) of the HF per-unit mass emitted by the larger pouch cells". This statement is incorrect. The 2017 Larsson Study does not even report HF emissions on a mass basis; in fact, it does not appear that Larsson et al. even reported the mass or weight of any of the batteries that were tested. This makes it impossible to "convert" the "cylindrical cells' HF emissions" to a "mass basis". The 2017 Larsson Study does not even recognize HF emissions on a "mass basis"; it only recognizes HF emissions on a "per Wh" basis.

Page 10: The developer's emission factor is conservative because it "inherently assumes a high degree of combustion of the BESS's battery mass, converting a significant fraction of the batteries' fluorine" into HF. To test the veracity of this statement, one must simply calculate the amount of HF that would be emitted if all the fluorine in the electrolyte of a PowerTitan 2 BESS were converted to HF and then compare this result to the 38.68 pounds of HF emissions that were input to the AERMOD analysis[14]. This calculation requires the following information:

A PowerTitan 2.0 BESS is 13.7% by weight $LiPF_6$[15].

A PowerTitan 2.0 BESS weighs 61,200 pounds[16].

A mole of $LiPF_6$ has six moles of fluorine (F).

A mole of HF has one mole of fluorine (F).

The molecular weight of $LiPF_6$ is 152 g/mole or 0.334 lb/mole.

The molecular weight of HF is 20.0 g/mole or 0.0440 lb/mole.

The first step is to calculate the number of moles of $LiPF_6$ in the electrolyte of a PowerTitan 2 BESS unit:

$$\text{Eq. 2} \qquad \frac{13.7\ lb\ \text{LiPF}_6}{100\ lb\ \text{of BESS}} \times \frac{61{,}202\ lb\ \text{BESS}}{\text{PowerTitan 2}} \times \frac{1\ mole\ \text{Li}PF_6}{0.334\ lb\ \text{Li}PF_6} = 2.51 \times 10^4\ moles\ \text{Li}PF_6\ \text{per PowerTitan 2}$$

The next step is to calculate the pounds of HF that would be emitted if all the $LiPF_6$ in a burning PowerTitan 2 BESS were converted to HF:

[14] The spreadsheet on page 1 of Attachment A included in the developer's response to Data Request 6 states that the total HF emissions from the combustion of a PowerTitan 2 BESS is 38.68 pounds.
[15] Per the Safety Data Sheet (SDS) provided by SunGrow; see Data Request Response #2 part 6.
[16] Per Page 1 of Attachment A in the developer's response to Data Request #6.

Eq. 3 $$\frac{2.51 \times 10^4\ moles\ \mathrm{LiPF_6}}{\text{PowerTitan 2}} \times \frac{6\ moles\ \mathrm{F}}{mole\ \mathrm{LiPF_6}} \times \frac{1\ mole\ \mathrm{HF}}{mole\ \mathrm{F}} \times \frac{0.0440\ lb\ \mathrm{HF}}{mole\ \mathrm{HF}} = \frac{6{,}630\ lb\ \mathrm{HF}}{\text{PowerTitan 2}}$$

As this equation demonstrates, if all the electrolyte in a PowerTitan 2 burned and all the fluorine in the electrolyte were converted into HF, then 6,630 pounds of HF would be emitted.

Nonetheless, the developer's AERMOD analysis assumes that only 38.68 pounds of HF will be emitted if a PowerTitan 2 is completely burned; this accounts for less than 0.6% of all the fluorine in the electrolyte:

Eq. 4 $$\frac{38.68\ lb\ HF\ emitted\ (according\ to\ developer)}{6{,}630\ lb\ HF\ emitted\ (if\ all\ electrolyte\ fluorine\ converts\ to\ HF)} = 0.00583 = 0.583\%$$

These calculations show that the developer's HF emission factor accounts for only about a half percent of all the fluorine in the PowerTitan 2 electrolyte; they also show that the developer assumes 99.4% of the fluorine in the PowerTitan 2 electrolyte ***will not*** convert to HF even during a complete BESS fire event! Clearly, the developer's 38.68 pound HF emission factor ***does not*** assume "a high degree of combustion of the BESS's battery mass" and it certainly ***does not*** assume that "a significant fraction of the batteries' fluorine" is converted into HF. The developer's HF emission factor is decidedly not conservative and does not ensure a "health protective" assessment.

SORT does not contend that all of the fluorine in the electrolyte of a PowerTitan 2 BESS will form HF during a deflagration event; however, it is certain that some percentage electrolyte conversion to HF conversion will occur. If we assume that just 10% of the fluorine in the electrolyte converts to HF during the combustion of a PowerTitan 2, then 663 pounds of HF would be emitted. This is consistent with the 662 pounds of HF emissions that SORT projected in our scoping comments submitted March 4, 2026[17]. Moreover, if only 2% of the fluorine in the electrolyte were converted to HF (which is a *very* conservative assumption), it would still result in the release of 133 pounds of HF which is nearly 4 times higher than the paltry 38.68 pounds of HF emissions that were input to the developer's AERMOD assessment. All of this demonstrates that the developer's HF emission factor is not conservative; to the contrary, it is unreasonably low.

The insufficiency of the developer's HF emission factor can be further demonstrated by comparing the developer's HF emission factor to published HF emission factors. To draw this comparison, one must first convert the developer's calculated emission factor

[17] Page 12.

of 631.86 mg HF/kg battery into mg HF/Wh to make the units consistent with published HF emission factors:

Eq. 5 $$\frac{631.86\ mg\ \text{HF}}{kg\ \text{battery}} \times \frac{1\ kg\ \text{battery}}{2.2\ lb\ \text{battery}} \times \frac{61{,}202\ lb\ \text{battery}}{1\ \text{PowerTitan BESS}} \times \frac{1\ \text{PowerTitan BESS}}{5{,}010{,}000\ Wh} = 3.51\ mg\ \text{HF}/Wh$$

This 3.51 mg/Wh emission factor is ***absurdly*** low***;*** it is an order of magnitude less than most published HF emission factors and it is nearly 4 times smaller than the smallest HF emission factor published by the 2017 Larsson Study (which was 12 mg/Wh). In short, there is ***nothing*** conservative about the developer's HF emission factor:

- It assumes that 99.4% of the fluorine in a PowerTitan 2 BESS remains unaffected by a deflagration event.
- It is at least an order of magnitude smaller than published emission factors.
- It is based on substantially flawed HF emission data from the Liu Study.
- It assumes without evidence that HF emissions are a function of battery weight.

Page 10: The developer claims that the modeling parameters used in the AERMOD analysis "likely overstate the potential emissions" because the BESS will not fully burn, all safety systems will work properly, and the model does not account for HF adsorption or deposition. This argument is not persuasive. Even if only half a PowerTitan 2 burns, it will still release hundreds of pounds of HF and thus pose a significant toxic risk. Furthermore, control systems fail all the time, so it is highly imprudent to assume that none of the thousands of BESS units that will be installed by the developer will ever fail throughout the 30+ year life of the project. Finally, the space between the maximum exposed individual receptor and the nearest BESS unit is so small and so empty that there will be very, very little HF "adsorption" or "deposition".

Page 11: The developer argues that the HF emission factor is "on the high end of credible data for LFP" and is "several times higher than the HF yield measured in full-scale LFP module tests without flame ignition". None of these statements are correct. First, the developer does not even identify what study is meant by the "full-scale LFP module tests without flame ignition", so that claim must be rejected because its veracity cannot be assessed. Second, the developer's HF emission factor is not "on the high end" of any LFP test results; to the contrary, it is half of the average value projected by the flawed Liu Study in which HF emissions were substantially underreported.

Page 11: The developer states that using high-cobalt cell data to estimate emissions from an LFP BESS will greatly over-predict emissions beyond any credible level because Ramboll notes that taking the absolute maximum HF/HCl emission factors from disparate studies "over-predicts the emissions likely to occur at BESS facilities,

particularly those that employ LFP batteries." This is a strawman argument because nobody is suggesting that the developer use "absolute maximum" data from "high-cobalt cell" tests to calculate HF emissions for the PowerTitan 2 BESS. Furthermore, the developer misrepresents the Ramboll report which *actually* states on pages 12-13 that "We note that most of that literature evaluates fires from NMC batteries, which tend to burn at higher temperatures and experience higher rates of consumption. The emissions factors presented in this report are therefore conservative estimates that over-predict the emissions likely to occur at BESS facilities, particularly those that employ LFP batteries". Here, the Ramboll report merely points out that using NMC data will overpredict LFP emissions; it says nothing about "absolute maximums" or "disparate studies". Additionally, Ramboll's HF emission factor of 11,320 mg/kg of battery weight was established based on LFP data, not NMC or "high-cobalt" data[18]; thus, according to Ramboll's own premise, it is not highly "overpredictive". Moreover, the 11,320 mg HF/kg emission factor adopted by Ramboll is nearly twenty times higher than the 631.86 mg HF/kg emission factor assumed by the developer for the PowerTitan 2. This fact alone demonstrates that the developer's HF emission factor is clearly not conservative.

Page 11: The developer states that using data from the Liu study and then reducing it by another 50% "achieves a balance of realism and conservatism" because HF inputs are "high enough to cover severe failure conditions (full thermal runaway propagation with fire, all batteries involved)". This statement is factually incorrect. Intrinsic flaws and bias in the Liu Study data render the developer's HF emission factor substantially understated, and the application of an additional 50% correction factor further understates HF emissions. Additionally, the developer's HF emission factor does not cover "full failure conditions"; to the contrary, it assumes that 99.4% of the electrolyte in PowerTitan 2 BESS will remain unaffected even in a full deflagration event!

Page 11: The developer argues that the HF emission factor of 631.86 mg/kg is "grounded in a relevant large-scale experimental study (Liu et al. 2021)" and "adjusted using peer-reviewed findings (Larsson et al. 2014) to reflect the specific characteristics of the Project's LFP prismatic cells." SORT notes that, for the reasons provided above, the Liu Study is not an appropriate basis for the developer's HF emission factor because it openly admits that HF emissions were underreported. Furthermore, if the "peer reviewed" Larsson Study is of sufficient quality to derive a "correction factor", then it is also of sufficient quality to derive an "emission factor". The developer does not recognize this, and instead disregards the Larsson Study for the purposed of deriving an HF emission factor and instead relies solely on the substantially flawed Liu Study.

[18] See pages 43 and 46.

Page 11: The developer claims the HF emission factor is "intentionally conservative" and "chosen near the upper end of realistic emissions for LFP batteries and applied in conjunction with worst-case assumptions (complete container burn, no mitigation)". This statement is incorrect. The "upper end" of HF emission measurements in the Liu Study is 8.1 grams, but the developer's HF emission factor assumes only 5.45 grams; thus, the developer's assumption is nearly 35% less than the "upper end". Furthermore, the developer's HF emission factor does not represent a "complete container burn"; to the contrary, it assumes that 99.4% of the electrolyte in the PowerTitan 2 remains fully intact during a container burn event.

Page 11: The developer claims that the model overestimates potential emissions and concentrations. This statement is incorrect. The AERMOD results substantially underestimates HF emissions and concentrations because it assumes that 99.4% of the electrolyte in the PowerTitan 2 does not burn during a container burn event.

Page 11: The developer argues that robust scientific data and proven scaling adjustments provide confidence that the calculated emission factors provide a human health and environment-protective representation of a worst-case BESS thermal runaway/fire event. This statement is incorrect. The Liu Study upon which the developer's emission factor is based is not "robust"; it is deeply flawed and the authors themselves acknowledge that HF results are underreported. Furthermore, the modeled results do not represent a worst-case BESS fire event because they presume that 99.4% of the electrolyte in the PowerTitan 2 will not burn and will remain fully intact during a container burn event.

Page 11. The developer claims that the approach adopted for the BESS project is consistent with the CEC's guidance to use technically sound, peer-reviewed data, and to err on the side of over-predicting potential impacts rather than under-predicting them. This statement is incorrect. The developer's HF emission factor is derived from a flawed study that underreports HF emissions and incorporates an unreasonable 50% correction factor. Moreover, the developer's analysis does not overpredict potential impacts; to the contrary, it assumes that 99.4% of the electrolyte in the PowerTitan 2 will remain intact during a container burn event.

Note: This discussion focusses only on HF emissions even though the developer also addresses HCl emissions in the response to "Information Request 6". SORT does not have the bandwidth to analyze the developer's HCl arguments in detail. However, the developer's HCl emission factor is based on the Liu Study results; therefore, it is flawed for the same reasons that the HF emission factor is flawed[19]. Accordingly, the Commission should not accord weight to the developer's claimed HCl emissions.

[19] HCl is highly soluble and highly reactive; thus, it was underreported just as HF was underreported.

SORT DISPUTES THE RESPONSE TO "REQUEST FOR INFORMATION #8". SORT notes many deficiencies in the developer's response to Request for Information #8. For example, the developer states on page 13 that the Palmdale meteorological monitoring system is "managed and curated by the South Coast Air Quality Management District", and then states on page 14 that it is managed by the California Air Resources Board. Neither of these statements appear to be correct; in fact, Palmdale is not even in the South Coast Air Quality Management District. SORT understands that Palmdale weather station (KPMD) is located on U.S. Air Force Plant 42[20].

On pages 13 and 14, the developer devotes several paragraphs to explaining how AERMOD requires meteorological data to be in a certain format and requires surface characteristics to be properly described; these pages also explain how the EPA's AERMET and AERSURFACE programs can be used to put meteorological and surface data into the proper format. However, what the developer *does not* explain is why Acton weather data could not be put into the correct format using AERMET or why appropriate surface characteristics cannot be derived using AERSURFACE. There are many weather stations in Acton that provide windspeed, wind gust, wind direction, temperature, relative humidity and other parameters; these weather stations (most of which are owned and operated by Southern California Edison) have operated reliably for years and have robust wind histories. The developer does not identify any deficiencies in the completeness or quality of Acton weather data[21].

Instead of explaining why Acton weather data cannot be used for exposure modeling purposes, the developer argues that the AERMOD Implementation Guide does not require the "use of data from the closest meteorological station, particularly where such data does not meet completeness or quality requirements" and that the "use of a station with regulatory-grade representative data is standard practice, compared to using closer, non-compliant data that could underestimate or mischaracterize dispersion conditions". The problem is, the developer has not shown that Acton meteorological data does not meet "completeness or quality requirements" or is "non-compliant" or underestimates/mischaracterizes "dispersion conditions". Moreover, SORT does not believe that the developer can make such a such showing because Acton weather data is robust; it has to be because Southern California Edison relies on it for wildfire protection purposes. Equally important, EPA regulations require that meteorological inputs represent the modeled area and note that "geographical representativeness is best achieved by collection of all of the needed model input data in close proximity to the actual site of the source(s)" [40 CFR Appendix W to Part 51 § 8.4.4.1(a)].

---

[20] https://metar-taf.com/metar/KPMD#google_vignette

[21] Missing cloud cover or upper air data could be obtained from other weather stations in the area. This is reasonable, since the developer believes all the Palmdale data should be used.

Accordingly, the developer's AERMOD results cannot be deemed sufficient for assessing the public safety risks posed by the BESS project until the developer has conclusively proven that the Palmdale meteorological data upon which it is based accurately represents meteorological conditions at the project site in Acton.

On Pages 15-16, the developer describes Santa Clarita meteorological data and explains that the U.S. Geological Survey's National Land Cover Database was used for land cover inputs into AERSURFACE. Next, the developer mentions the Palmdale station and then discusses NOAA data and that upper air data is obtained from NOAA. The next paragraph again discusses the U.S. Geological Survey's National Land Cover Database and how it is used for inputs to the AERSURFACE model for albedo, Bowen ratio, and surface roughness. Then, the developer declares that "Acton does not produce data that meets the regulatory requirements". However, the developer does not identify the "regulatory requirements" which are not met by the Acton data. There is no reason why the developer can't source upper air data from NOAA or land cover inputs from the U.S. Geological Survey; if cloud cover data is missing, it could be sourced from Palmdale. The developer even admits that upper air data, albedo, Bowen ratio, and surface roughness at Acton are similar to the Palmdale Airport datasets.

At least the developer confirms that prevailing winds at the project site blow from the northeast. This means that, even using the developer's paltry 38.86 pound HF emission factor, it is likely that numerous residences located south and west of the project site (all of which are within 227 feet of a BESS) will experience HF concentrations that exceed the established safety threshold when a BESS deflagration occurs. The developer dismisses this discrepancy by arguing "wind direction is not the only factor that defines whether a meteorological dataset is representative or not". However, wind direction was the determining factor for selecting the MEIR location and is therefore a critical element of the AERMOD results. In fact, page 6 of the Response to Data Request #6 states that the MEIR was located northeast of the BESS yard because it "corresponds to the nearest residential land use downwind of the BESS under predominant wind conditions". Of course, the predominant wind direction at the project site ***is not*** from the southwest; therefore, the MEIR is probably not northeast of the BESS yard.

The developer then states "Absent an on-site or regulatory-approved meteorological dataset in Acton, the Palmdale Airport and Santa Clarita datasets are most appropriate for use in modeling emissions at the Project site". This statement is incorrect. First, AERMOD ***does not require*** "regulatory approved meteorological datasets"; to the contrary AERMOD clearly authorizes "site specific" and custom data sets[22]. Site specific

[22] 40 CFR Appendix W to Part 51 § 8.4.4.1. https://www.epa.gov/scram/meteorological-processors-and-accessory-programs

data sets just take more work because they have to be set up. Second, the Palmdale Airport dataset clearly does not represent meteorological conditions at the project site because the Palmdale wind direction is completely wrong. While other factors in Acton such as albedo, upper air data, Bowen ratio, and surface roughness may be similar to Palmdale, if wind patterns differ substantially, then the meteorological data ***does not*** represent site conditions. Third, because the Palmdale dataset does not represent the project site conditions, it is ***not*** the most appropriate for "modeling emissions at the project site".

Finally, the developer claims that the Palmdale dataset is appropriate because "there are receptors on the northern and southern boundaries of the Project site". This claim ignores two important points. First, the Palmdale dataset set is not appropriate because it does not represent conditions at the project site. This is a fundamental principle of dispersion modeling and the developer knows it because page 13 states "Appendix W requires that meteorological data be representative of conditions affecting the source and receptors". Second, there are more and closer receptors on the south and western boundaries of the project site; thus, it does seem rather important that these receptor locations be assessed.

CONCLUSION

SORT respectfully requests that the Commission consider the information provided herein in the contemplation of the proposed BESS project.

Sincerely;

/S/ Jacqueline Ayer
Jacqueline Ayer, Director,
Save Our Rural Town

ATTACHMENT 1.

HYDROGEN FLUORIDE EMISSIONS FROM LITHIUM-ION BATTERIES DURING INDUCED THERMAL RUNAWAY VIA IN SITU LASER SPECTROSCOPY BY YI YAN, NICOLAS S.B. JAEGER, AND R. MITCHELL SPEARRIN (UCLA STUDY).

Proceedings of the Combustion Institute 41 (2025) 105800

Contents lists available at ScienceDirect

Proceedings of the Combustion Institute

journal homepage: www.elsevier.com/locate/proci

Hydrogen fluoride emissions from lithium-ion batteries during induced thermal runaway via in situ laser spectroscopy

Yi Yan *, Nicolas S.B. Jaeger, R. Mitchell Spearrin

Department of Mechanical and Aerospace Engineering, University of California, Los Angeles (UCLA), Los Angeles, California, 90095, USA

ARTICLE INFO

Keywords:
Lithium-ion battery fire
Hydrogen fluoride emissions
Tunable diode laser absorption spectroscopy
Fire dynamics

ABSTRACT

Improved understanding of hydrogen fluoride (HF) emissions from lithium-ion battery fires, including the temporal dynamics, is needed to optimize fire response and protection. Due to the high polarity of HF and its associated surface adsorption and reactivity, most traditional sensing methods are prone to error and slow response due to issues with sampling or surface interactions. To address these limitations, an in situ tunable diode laser absorption spectrometer is developed to achieve real-time measurements of HF emissions during dynamic battery fires with a temporal resolution of milliseconds, and with detection limits of single parts per million along with several orders of magnitude of dynamic range. The laser spectrometer is used in situ to perform measurements near the fire source so that the fire dynamics and the transient behavior of HF emissions can be more accurately characterized. Thermal runaway and fire/explosion conditions of model 18650 lithium-ion batteries are simulated in a conical radiative heater, and HF measurements are performed online via an optical access port in the effluent exhaust. By varying the radiative heating flux of the conical heater and the initial state of charge of the batteries, different characteristics of the safety venting and thermal runaway behavior of lithium-ion batteries and the corresponding emissions of toxic HF gas are measured. These findings provide valuable insights into the dynamics of lithium-ion battery fires and will aid in the development of strategies to mitigate their associated risks.

1. Introduction

The increasing reliance on lithium-ion (Li-ion) batteries in consumer electronics, electric vehicles, and other energy storage systems has raised significant concerns regarding their safety. The risks associated with Li-ion batteries stem from their high energy density and the potential for thermal runaway, a self-propagating process initiated by exothermic reactions within the cell. This process can lead to hazardous gas emissions, fire, and explosions. The progression of thermal runaway can generally be divided into several distinct stages. The initial heat-up stage occurs when external mechanical, thermal, and electrical abuse causes the battery temperature to rise. As external heating progresses, the battery transitions to the onset of a self-heating stage (T_o), triggering exothermic reactions between the electrolytic fluid and charged anode, leading to further temperature increases until the battery reaches the rapid thermal runaway threshold (T_r). In the rapid thermal runaway stage, the complete breakdown of electrolytic barriers causes highly exothermic reactions with oxidizers inside the battery or ambient air, driving an abrupt and exponential temperature rise until reaching a local maximum temperature (T_m) [1,2]. An additional intermediate stage, known as the safety venting stage, has also been reported in certain studies on cylindrical and prismatic Li-ion cells [3,4]. In this stage a burst of gas emission occurs before the onset of thermal runaway due to a rupture of the battery's venting disk at a lower temperature (T_v), a safety design feature intended to relieve internal pressure. Battery thermal runaway is influenced by multiple factors, including state of charge (SOC), battery chemistry, and environmental conditions. The release of gas emissions during the various stages of the battery progression to thermal runaway can serve as an important indicator for safety and fire management.

Previous studies have extensively examined temperature evolution and gas emissions during thermal runaway using thermocouple measurements and gas sampling-based techniques, with notable limitations. First, gas sampling methods for ex situ analysis, such as Fourier Transform Infrared Spectroscopy (FTIR) and gas chromatography, suffer from slow response times and low temporal resolution relative to the fast transient events of a Li-ion battery fire [3,4]. Second, the remote location of the analytical instruments and requisite sampling leads to adsorption and surface reaction losses of less stable species along the sampling lines (on top of the additional measurement latency and sample dispersion). This introduces measurement inaccuracies, particularly

* Corresponding author.
E-mail address: yydjx@ucla.edu (Y. Yan).

https://doi.org/10.1016/j.proci.2025.105800
Received 22 April 2025; Accepted 25 July 2025
Available online 18 August 2025

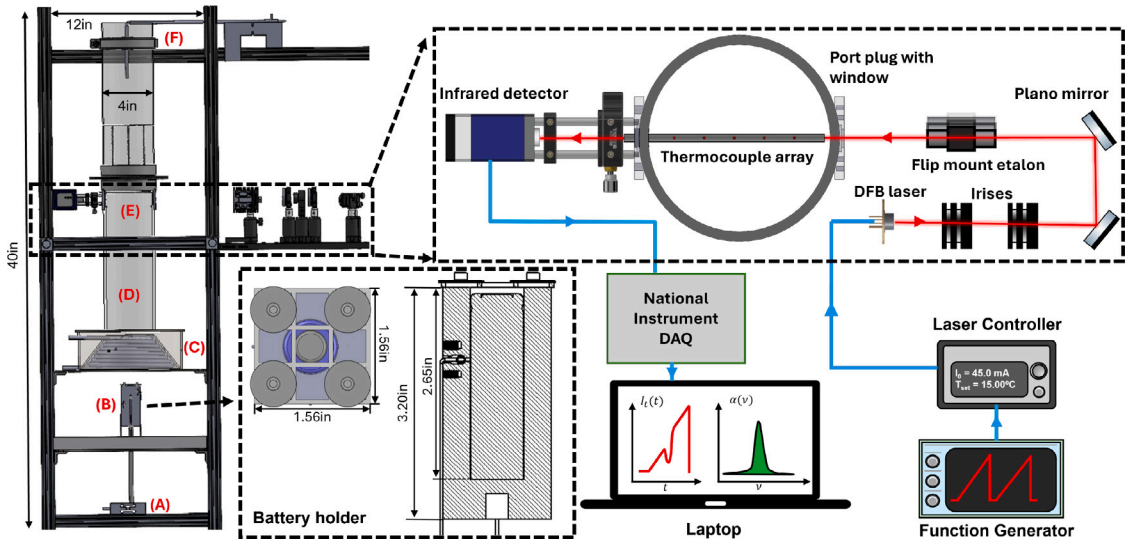

Fig. 1. Schematic of the experimental setup. *Left:* Radiative heater facility includes (A) single-point load cell, (B) battery holder, (C) conical heating element, (D) gas exhaust duct, (E) gas test section with LAS setup, (F) pitot-thermocouple velocimeter. *Bottom Middle:* Top view and side view cross-section of battery holder with a testing Li-ion battery inserted. *Top Right:* LAS optical components and electronics.

in the case of reactive gas species such as hydrogen fluoride (HF).

Hydrogen fluoride is among the most toxic byproducts of Li-ion battery thermal runaway, with health impacts including pulmonary inflammation, dermal burns, and systemic toxicity [5]. When Li-ion batteries experience external abuses such as external heating, hydrogen fluoride is primarily generated from the decomposition of the electrolyte salt ($LiPF_6$) and the fluorinated polymer binder (PVDF), which degrade at different temperature ranges [6]. These decomposition pathways result in distinct HF emission characteristics due to different electrochemical reactions and associated activation energies [7–9], with the key global reaction equations in (1)–(5). As indicated, the high electronegativity of fluorine effectively abstracts hydrogen from water and other species to form HF.

$$LiPF_6 \longrightarrow LiF + PF_5 \quad (1)$$

$$PF_5 + H_2O \longrightarrow POF + 2\,HF \quad (2)$$

$$LiPF_6 + H_2O \longrightarrow LiF + POF_3 + 2\,HF \quad (3)$$

$$POF_3 + H_2O \longrightarrow POF_2(OH) + HF \quad (4)$$

$$-CH_2-CF_2- \longrightarrow -CH{=}CF- + HF \quad (5)$$

Due to the high polarity of hydrogen fluoride and its tendency to adhere to and react with surfaces, accurately quantifying HF emissions remains a significant challenge in fire safety research. Most previous studies have relied on indirect or delayed measurement methods, leading to potentially errant measurements of HF concentrations [10,11]. To overcome these limitations, this study employs in situ laser absorption spectroscopy (LAS) to enable online, high time-resolution measurements of HF emissions during Li-ion battery fires. LAS offers highly quantitative in situ optical detection with kHz time resolution, eliminating sampling line losses and measurement latency. We use a radiative heater to induce controlled thermal runaway conditions for cylindrical 18650 Li-ion batteries under varying SOC conditions. The high-speed in situ HF measurements obtained in this study provide critical insights into HF emission dynamics, improving the understanding of Li-ion battery fire hazards and informing fire protection strategies.

2. Methods

2.1. Experimental facility and instrumentation

To investigate Li-ion battery fires under controlled thermal abuse conditions, a radiative heating experiment was constructed (Fig. 1. *Left*). A single cylindrical Li-ion battery (Sanyo NCR 18650 GA) was positioned vertically in a custom-designed battery holder (Fig. 1(B)) and subjected to blackbody radiation via a conical heating element (Fig. 1(C)). The battery state of charge preparation followed the methods and procedures described in [2] to ensure consistency and repeatability across tests. The battery holder was mounted on a single-point load cell via a ceramic connecting rod (Fig. 1(A)) to continuously monitor battery mass loss during testing. To track the thermal response of the battery, two spring-loaded thermocouples were installed in direct contact with the battery surface through the battery holder walls. During the experiment, gaseous battery emissions from venting and thermal runaway were directed through an exhaust duct (Fig. 1(D)), which included a designated test section that is optically accessible (Fig. 1(E)), such that gas properties could be measured in situ using a laser absorption spectrometer (Fig. 1 *Top Right*) and the temperature of the gas was determined using a thermocouple array (TC array) with five thermocouples installed 0.5 inches above the laser path. As the sample gas moves further along the exhaust duct, it passes through a flow conditioner, ensuring a more uniform flow profile before reaching the pitot-thermocouple velocimeter (Fig. 1(F)) that provides an exhaust gas flow rate measurement, allowing for the total mass of HF emitted to be determined. All measurement signals, except for the LAS detector output, were recorded using two synchronized data acquisition devices (DATAQ DI-2008) at a sampling rate of 33 Hz. The LAS detector signal was acquired separately using a high-speed data acquisition device (NI-PXI 6115) with a sampling rate of 400 kHz, enabling high-resolution spectral analysis.

2.2. Controlled battery heating rate

A coiled 3.55-meter-long Incoloy 800 conical heater (5 kW maximum power), controlled via surface temperature feedback, was employed to deliver radiative heating flux to the test battery. The surface heating flux on the top plate of the battery holder was measured by a heat flux gauge. Given the vertical orientation of the battery, and relatively small exposed area, direct radiative heating was somewhat secondary, and the primary heat transfer to the test battery occurred through thermal conduction via the larger battery holder, which was heated by the radiation source and internal reflections from radiation shielding in the test chamber. To further quantify the effective thermal energy gain to the test battery, the rate of battery temperature increase during the linear heat-up phase, prior to the onset of safety

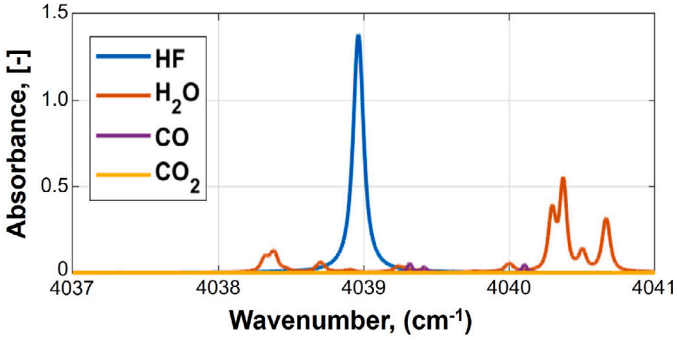

Fig. 2. Simulated target transitions of major gas products during battery fire at gas temperature of 1800 K, including HF (X_{HF} = 1%), H_2O (X_{H_2O} = 15%), CO (X_{CO} = 30%), and CO_2 (X_{CO_2} = 40%).

venting, was also measured. This temperature gradient served as an indirect metric for assessing the net energy absorbed by the battery under different heating conditions. Three different heater temperature setpoints were selected to produce distinct battery surface temperature ramp rates. These conditions were designed to align with the three thermal runaway propagation behaviors identified in [12], and enabled a systematic investigation of how heating rate influences HF emissions dynamics and thermal runaway behaviors.

2.3. HF laser absorption spectroscopy

The mole fraction of HF in the test section was measured using a tunable diode laser absorption spectroscopy (TDLAS) setup. A distributed feedback (DFB) diode laser (Norcada NL2475) was used to target the R(1) rovibrational transition of HF at 4038.965 cm^{-1} in the fundamental band of HF [13] over a 4 inch optical path length across the exhaust duct above the heater. A laser controller (Arroyo 6305) was used to set the laser chip temperature and the injection current, which was modulated with a 1 kHz linear ramp function from a function generator (Rigol DG1032Z) to achieve wavelength tuning across the absorption line of HF. After passing through the sample gas, the transmitted laser beam is detected and conditioned by a VIGO photovoltaic detector (MIP-DC-50M-F-M8) and recorded on an external data acquisition device (NI-PXI 6115) at a 400 kHz sampling rate.

In this study, the LAS sensor was scanned in wavenumber from 4037.5 cm^{-1} to 4041 cm^{-1}, which fully captures the selected HF spectral line and neighboring features as shown in Fig. 2. Within this spectral range, several water vapor absorption transitions from E'' = 1581–4728 cm^{-1} are also active at high temperatures, providing an alternative means for optical gas temperature measurement based on the Boltzmann intensity distribution. Other major combustion gas species, such as CO and CO_2, are shown to have negligible interference with the target HF line, per Fig. 2. During Li-ion battery fires, a certain amount of volatile hydrocarbons are generated [14], but their C-H vibrational modes do not fall in the spectral range of this study. One representative laser intensity scan highlighting the resolved lines during a battery fire test is shown in Fig. 3 (*top*). The corresponding absorbance spectrum was calculated via $\alpha_\nu = -\ln\left(I_t/I_0\right)_\nu$ where I_t and I_0 represent the transmitted and incident intensities of the laser light, respectively. The absorbance spectrum was then integrated using $\int_\nu \alpha_\nu = S(T)X_i PL$ to determine the HF mole fraction, where $S(T)$ is the spectral linestrength, P is the gas pressure, L is the laser path length, and X_i is the gas mole fraction. To recover the integrated absorbance areas, the spectrum for each scan was fitted using Voigt lineshape profiles and line parameters from the HITRAN database as shown in Fig. 3 (*bottom*), allowing for the simultaneous retrieval of gas temperature, HF mole fraction, and water vapor mole fraction [15,16].

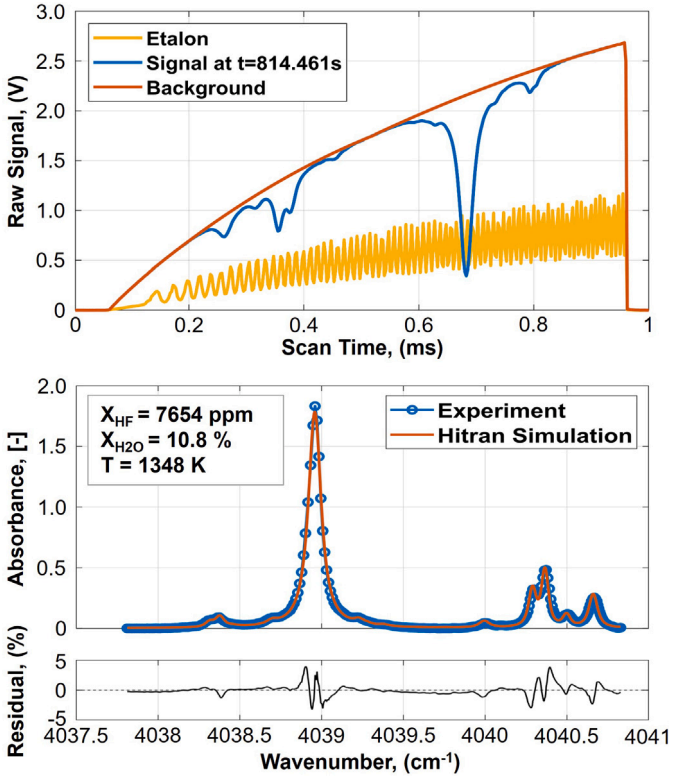

Fig. 3. *Top*: Instantaneous light absorbance signal during battery fire event. *Bottom*: Spectral fit of the instantaneous signal with the HITRAN database for gas properties measurement.

2.4. Exhaust gas measurement

The exhaust gas temperature and velocity were measured to characterize gas dynamics and mass flow rate during the battery fire events. The flow velocity was determined using a pitot-thermocouple velocimeter, while the gas temperature was recorded by a thermocouple next to the pitot tube. The calculation of exhaust gas velocity was based on $v_{\text{gas}} = K\sqrt{\frac{2\Delta P_{\text{gas}}}{\rho_{\text{gas}}(T_{\text{gas}})}}$, where ΔP_{gas} is the pressure difference between stagnation and static pressure, $\rho_{\text{gas}}(T_{\text{gas}})$ is the temperature-dependent gas density, and the K factor is an empirically derived correction coefficient, calibrated to be 1.025. The mass flow rate was then determined using $\dot{m}_{gas} = \rho_{gas}(T_{gas}) \cdot v_{gas} \cdot A_{tube}$.

The exhaust gas temperature (T_{gas}) measurement was corrected based on the energy balance of the thermocouple bead according to [17]. In this study, potential heat losses due to conduction and radiation are expected to be minimal, owing to the small size of the thermocouple bead and its supporting tube, as well as the relatively small temperature difference between the bead and the thermally insulated surrounding walls. Therefore, the updated correction relation from [17] only counts for the convection effect using $T_{\text{gas}} - T_{\text{TC}} = \frac{\rho_{\text{TC}} C_{p,\text{TC}} D}{4h}\frac{\partial T_{\text{TC}}}{\partial t}$ where ρ_{TC} and $C_{p,\text{TC}}$ are the density and specific heat capacity of bead material, respectively, and h is the convective heat transfer coefficient. The value of h was evaluated using Whitake's empirical correlation [18].

3. Results

In this study, nine battery thermal abuse tests with three different battery states of charge (100%, 50%, and 0%) were conducted at three levels of radiative heating power yielding distinct levels of equilibrium battery temperature gain rates of approximately 21.3 K/min, 12.8

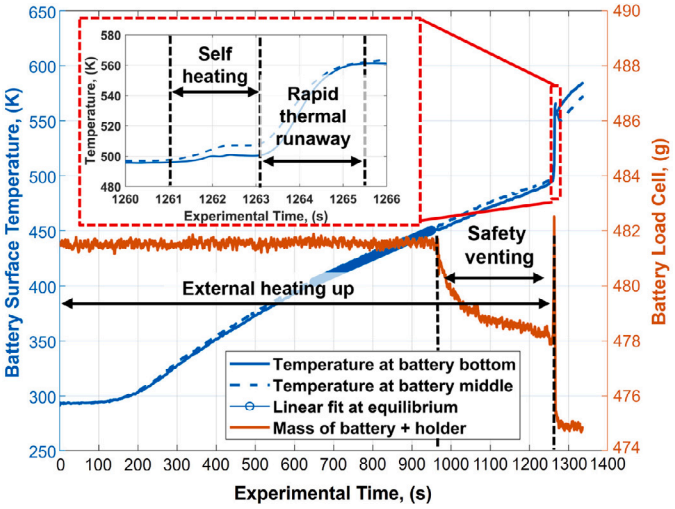

Fig. 4. Temperature and mass measurement of the battery (and holder) over the experiment period with the illustration of four stages during a Li-ion battery fire.

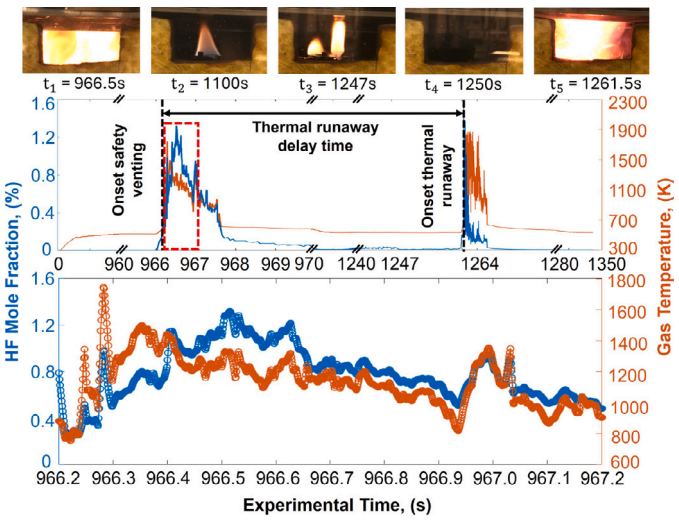

Fig. 5. HF emission and fire evolution. *Top*: Instantaneous picture frames of test battery during fire events. *Middle*: HF mole fraction and temperature of emission gas at test section over the experiment period. *Bottom*: zoomed window of gas mole fraction and temperature during dynamic period of safety venting.

K/min, and 7.6 K/min corresponding to the measurement in different thermal runaway propagation processes in [12]. To facilitate discussion of the typical battery fire events and gas emission dynamics, a representative experiment with a partially charged battery (50% SOC) under a heating flux of 36 kW/m^2 is highlighted in Figs. 4–6 and discussed in the following subsections.

3.1. Battery temperature and mass evolution

At the onset of heating, the battery temperature initially rises slowly due to the thermal inertia of the holder (and battery) and uneven heat distribution. After this initial phase (around 300 s in Fig. 4), the temperature rise gradient becomes semi-constant during a linear heat-up stage, until reaching T_o = 498 K at 1261 s, marking the onset of the self-heating stage, in which the battery temperature increased faster than the externally driven rate. Approximately two seconds after onset, the rapid thermal runaway threshold was reached (T_r = 504 K). This final stage was characterized by an accelerated mass loss due to electrolyte vaporization and venting as well as a sharp temperature increase that reached a local maximum of T_m = 561 K, accompanied by the violent rupture of the battery's internals and the expulsion of hot gases leading a sharp spike downward force on the battery load cell. Additionally, a significant precursor mass loss event was observed at t = 965.7 s and T_v = 455 K, corresponding to the safety venting stage reported in previous studies [3,4]. During this stage, the venting disk ruptured, releasing gaseous decomposition products prior to thermal runaway. Notably, the accumulated mass loss during venting was comparable to, or even higher than, that which was observed during thermal runway stages, but this mass loss occurred at a slower rate.

3.2. HF emission dynamics and battery fire evolution

To further analyze the fire dynamics, real-time HF mole fraction measurements were obtained using in situ laser absorption spectroscopy (LAS). A representative temperature and HF mole fraction evolution in the exhaust over the experiment period is shown in Fig. 5 (*Middle*), alongside time-synchronized frames from a video recording of the experiment to better visualize the fire progression (*Top*). Two distinct spikes in HF emissions were detected with mole fraction value over 1%, corresponding to the onset of safety venting (t_1) and the onset of thermal runaway (t_5). During the first fire event, a visible flame was present, accompanied by significant HF emissions. Although this flame weakened over time (t_2), it stabilized for an extended period (minutes), suggesting that hot electrolyte vapors were continually released and oxidized. As the fire progressed, the weak flame became unstable (t_3) and temporarily extinguished (t_4). The battery fire was reignited about 15 s later (t_5), leading to a second, more intense fire event. This secondary fire was significantly stronger with visible hot metal sparks, and coincided with a higher HF emission peak and a sharper temperature increase. Unlike the second fire event, which required higher temperatures to breach additional internal barriers, the fire in the safety venting stage was not detected by the battery surface temperature measurement, similar to past studies [2]. This is presumably because the flame in the venting stage was well-ventilated and did not cause the self-heating of the battery itself, making it difficult to capture using thermocouple measurements on the battery surface. While battery surface temperature measurements were insufficient to fully capture the fire dynamics, gas-phase temperature measurements provide a more direct method for characterizing the fire intensity in the test section. However, accurately capturing these fast-changing gas temperatures presents its own set of challenges. A common challenge in fast dynamic temperature measurements using thermocouples is their slow response time as mentioned in the previous section, often leading an underestimate of gas temperature even with the thermocouple correction approach [17]. To overcome this limitation, LAS thermometry was employed for more accurate measurement of gas temperature (when the water lines become sufficiently strong above 600 K) and HF gas mole fraction as shown in Fig. 5 (*Bottom*), benefiting from a response time over two orders of magnitude faster than the thermocouples (1 ms in LAS versus seconds in TC array).

3.3. Hydrogen fluoride production

While assessments based on mole fraction can provide insight into local gas concentrations, they are heavily influenced by ventilation conditions and the size of the surrounding environment, making direct comparisons across different fire scenarios challenging. In contrast, mass-based quantification provides a scalable and environmentally-independent measurement of toxic emissions, offering a more reliable approach to hazard assessment. Accumulated HF emissions on a mass basis were calculated from HF mole fraction and exhaust gas mass flowrate measurement. As shown in Fig. 6, The total HF production during the safety venting stage was about 124 mg which is about three times larger than the HF production during the thermal runaway stage

Table 1
18650 Li-ion battery thermal abuse experiment test results.

dT/dt (K/min)	SOC (%)	Onset temp.		Battery WL		TR delay (s)	Peak HF emi.		Accumulated HF emi.			
		SV (K)	TR (K)	SV (g)	TR (g)		SV (%)	TR (%)	SV (mg)	TR (mg)	Total[1] (mg/Wh)	Total[2] (%)
23.6	100	447	512	2.2	25.3	233	2.74	6.69	196	54	22.4	0.91
21.7	50	458	540	2.3	18.4	256	3.13	1.63	174	23	17.7	0.95
18.7	0	491	595	4.6	0.8	356	8.51	0.10	182	18	17.9	3.70
14.0	100	432	481	2.1	26.5	248	1.80	3.73	122	18	12.6	0.49
12.6	50	455	498	3.3	3.6	295	1.52	1.54	124	40	14.2	2.41
11.7	0	476	681	5.5	0.4	NA	2.58	0.05	117	12	11.6	2.19
7.68	100	427	478	3.4	25.2	320	0.08	4.66	69	27	8.65	0.34
7.50	50	437	493	3.5	7.7	456	0.30	1.82	31	21	4.59	0.46
7.56	0	453	658	5.3	0.8	NA	0.35	0.02	51	3.7	4.87	0.89

Total[1] is the total HF emission weight from safety venting (SV) and thermal runaway (TR) over full battery energy.
Total[2] is the total HF emission over the total battery weight loss (WL).
NA in thermal runway (TR) delay time indicates the onset of TR triggered at higher heating flux.

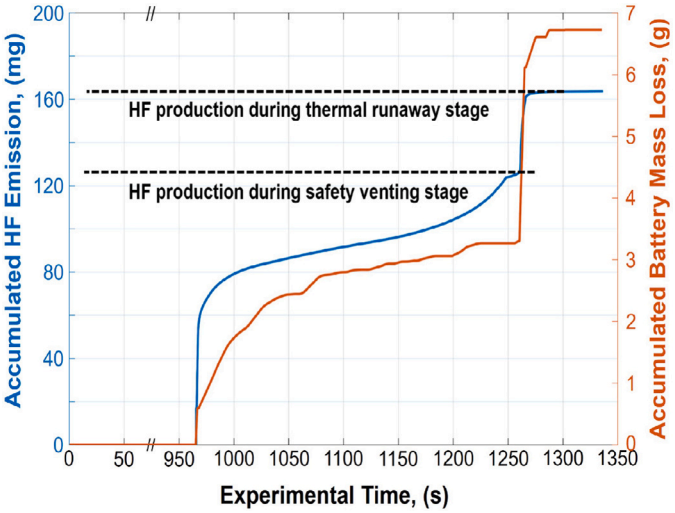

Fig. 6. Accumulated total HF mass production and the battery mass loss over the experiment period.

(40 mg in this specific case). Notably, a significant amount of HF was generated during the latter period of the gas venting stage (from t_2 to t_5 in Fig. 5). In contrast with the larger amount of HF produced in the safety venting stage, the battery mass loss experienced a more pronounced spike during the thermal runaway stage.

4. Discussion

Battery fire characteristics from the test series, including key emission metrics, are summarized in Table 1. The comparative results include initiation temperature of safety venting and thermal runaway, thermal runaway delay time with respect to the onset time of safety venting, peak HF emission, stage-specific HF mass production, and HF production normalized by battery energy capacity and battery mass loss. Trends in the dataset with respect to battery heating rate and state of charge are discussed in this section.

4.1. Onset temperature

The onset temperatures of battery fire stages of safety venting and thermal runaway ranged from 415 K to 492 K and from 461 K to 681 K, respectively. Both ranges fall within the findings reported in prior work [2,3]. With an increase of SOC level, both onset temperature values decrease due to the greater availability of internal electrochemical energy. With a higher heating flux, both onset temperatures measured on the battery surface increase likely due to greater thermal gradients between the battery surface and core, providing that each electrochemical reaction ignition temperature is consistent across different external heating fluxes. The gap between the safety venting and thermal runway onset temperatures becomes smaller at higher SOC levels as more energy is available to quickly transition from safety venting to thermal runaway.

4.2. Thermal runaway delay time

Based on the fast response and high time-resolution of the in situ HF LAS detection system, distinct spikes in emissions are observed to correspond to safety venting and thermal runaway, and thus a delay time between the two events can be well-quantified. This highlights the potential for a real-time HF spectrometer to provide forewarning of the more explosive thermal runaway event. At a constant heat flux, the thermal runaway delay time with respect to safety venting decreases with increasing SOC. This is because higher SOC levels contain more electrochemical energy, which accelerates the reactions leading to thermal runaway. At a constant SOC, increasing the heating flux also reduces the delay time, as it causes the battery temperature to rise more quickly and reach the reaction threshold sooner. A special case at 0% SOC was observed that at applied heating flux values of 27 and 36 kW/m^2, the 0% SOC battery only exhibited safety venting fire without progressing to thermal runaway. This suggests that there was insufficient energy input — both electrochemical (internal) and thermal flux (external heat) — to trigger the full runaway reactions. Thermal runaway was eventually observed at 0% SOC when a higher heating flux (53 kW/m^2) was applied.

4.3. Battery weight loss

The battery weight loss characteristics generally align with different major electrochemical reactions at varying activation temperatures, and appear consistent with prior work [6]. These physical trends in mass loss are discussed briefly here to provide context for subsequently discussed HF emissions trends. In general, as battery temperature increases, electrolyte decomposition and partial combustion occur first. The extent of this first-stage combustion is influenced by the onset temperature of safety venting. In the thermal runaway stage, higher temperatures can lead to non-reaction solid particle expulsion associated with over-pressurization of the battery structure, causing significant additional weight loss. Accordingly, in this study, across all SOCs and heating fluxes, weight loss during thermal runaway is higher than during safety venting. Between 50% and 100% SOC, venting-related weight loss is similar, but thermal runaway involves more intense

solid-particle expulsions at 100% SOC, resulting in greater weight loss. At 0% SOC, venting-related weight loss is larger than in the other SOC cases. With low electrochemical energy, combustion relies more heavily on external heating, resulting in more complete hydrocarbon fuel combustion with delayed over-pressurization. Due to the absence of significant energy to help drive reactions and explosive behavior, the thermal runaway stage causes minimal additional weight loss at 0% SOC.

4.4. HF emission concentrations

The peak concentration of HF emissions reached several percent in mole fraction, which is two orders of magnitude higher than values reported in existing literature [10]. This discrepancy is likely due to the high temporal resolution of LAS measurements, which accurately captures transient emission peaks, as well as the direct in situ measurement approach, which eliminates potential gas losses caused by adsorption or surface reaction inside the sampling lines. These factors contribute to a more accurate quantification of HF emissions compared to traditional gas sampling approaches and gas analysis techniques. HF measurement uncertainty was estimated to be 10% using the methods of [19]. A higher HF mole fraction peak was observed at higher SOC and higher heating flux presumably due to more internal electrochemical energy and stronger external thermal energy gain accelerating the HF production reactions. Comparing the safety venting and thermal runaway stages, the instantaneous HF mole fractions were either similar or higher during the thermal runaway stage, likely due to less total gas being generated. As will be discussed in the following sub-section, the metric of mole fraction alone in the evaluation of effluent toxicity can be misleading, especially in large scale fire accidents or with well ventilated conditions.

4.5. HF mass production

To quantify fire toxicity and exposure risk within a given spatial domain or volume, mass-based production from fire effluents is more relevant than instantaneous concentration [5], given that mass production of fire effluents is very dynamic. In this study, the total HF mass production from the batteries ranged from approximately 50 mg to 250 mg (Table 1). Given the full charge energy rating of 11.55 Wh, the total HF generation per unit energy capacity in this study ranged from 4.6 to 22 mg/Wh. This variation aligns with or falls near previously reported values [3]. The total HF mass generation per unit mass loss of the battery was also calculated in a wide range of 0.34% to 3.7% depending on the amount of total battery material loss from the thermal runaway stage. Notably, as shown in the example test in Fig. 6, and across other conditions as seen in Fig. 7, HF emissions production is consistently higher during the safety venting stage than during thermal runaway. This is because the primary source of HF is electrolyte decomposition, which occurs at relatively low temperatures. In contrast, HF generated during thermal runaway results mainly from the pyrolysis of fluorinated protective materials, which requires much higher temperatures. As also shown in Fig. 7, the total HF emission mass production (at a constant SOC) increases with heating rate while being weakly dependent on state-of-charge. The total HF emission does not vary significantly across different SOCs because the electrolyte and fluoride binder material are conserved in weight. However, lower external heating flux levels would lead to a decrease in total HF generation likely because the intermediate fluoridated gas species such as PF_5, POF_3, generated from electrolyte decomposition reactions (1) and (3) were emitted before their subsequent hydrolysis reactions (2) and (4) which require a higher temperature.

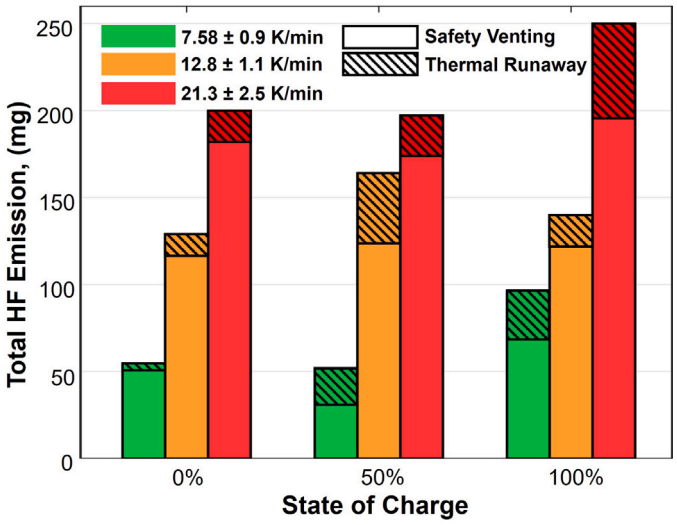

Fig. 7. HF mass production in safety venting stage and thermal runaway stage with different heating gain rate, and state of charge level.

5. Conclusions

This study examined Li-ion battery thermal abuse under controlled heating conditions, with a particular focus on HF emissions. Under varying heat input power and battery state of charge, we quantified the dynamics of thermal runaway and gas venting through time-resolved measurement of battery temperature, battery mass loss, gas temperature, and HF emissions. The latter element represents a novel implementation of in situ laser absorption spectroscopy for high-speed time-resolved HF emission measurements, which have proven difficult to acquire with traditional instrumentation. The high temporal resolution (1 kHz) of the LAS system in this study enables online monitoring of rapid off-gassing events, capturing transient emission spikes, and quantifying emissions production at different stages of the battery fire. This novel approach provides more accurate emission quantification and fire dynamics characterization.

The time-resolved HF emission measurements helped elucidate the two distinct emissions events during a Li-ion battery fire: the safety venting stage and the rapid thermal runaway stage. While the thermal runaway stage has been extensively studied due to its explosion hazards, this work illustrates the significance of the venting stage, as it can contribute to a substantial portion of toxic HF emissions. The study reveals that HF release during the early safety venting stage can significantly exceed emissions observed during thermal runaway. Overall, the findings offer valuable insights into battery fire dynamics and toxic gas exposure risks that are important for developing safer energy storage technologies and fire response protocols.

Novelty and significance statement

This study presents the novel application of in situ tunable diode laser absorption spectroscopy (LAS) for highly time-resolved quantification of hydrogen fluoride (HF) emissions during induced lithium-ion battery thermal runaway, addressing gaps in fire safety knowledge due largely to insufficient instrumentation to quantify hydrogen fluoride. By synchronizing LAS with controlled radiative heating experiments across varying states of charge (SOC), this study characterizes two distinct periods of HF emissions associated with safety venting and thermal runaway stages during a lithium-ion battery fire, and quantifies the cumulative HF emissions from each period. This integrated experimental facility and diagnostic method provides unique information for numerical model development and validation as well as new insights for fire response and management.

CRediT authorship contribution statement

Yi Yan: Designed and performed this research experiment, analyzed the data, and wrote the paper. **Nicolas S.B. Jaeger:** Designed the experiment, provided suggestions on data analysis, and reviewed and revised the manuscript. **R. Mitchell Spearrin:** Designed the experiment, provided comments and suggestions on experiment performance and data analysis, reviewed and revised the manuscript.

Declaration of competing interest

The authors declare that they have no known competing financial interests or personal relationships that could have appeared to influence the work reported in this paper.

Acknowledgment

The authors of this paper acknowledge that funding for this research was provided by the U.S. Federal Emergency Management Agency (Grant Number: EMW-2021-FP-00199).

References

[1] O. Willstrand, M. Pushp, P. Andersson, D. Brandell, Impact of different Li-ion cell test conditions on thermal runaway characteristics and gas release measurements, J. Energy Storage 68 (2023) 107785.
[2] A.W. Golubkov, D. Fuchs, J. Wagner, H. Wiltsche, C. Stangl, G. Fauler, G. Voitic, A. Thaler, V. Hacker, Thermal-runaway experiments on consumer Li-ion batteries with metal-oxide and olivin-type cathodes, RSC Adv. 4 (7) (2014) 3633–3642.
[3] L. Lin, O.A. Ezekoye, Time-resolved characterization of toxic and flammable gases during venting of Li-ion cylindrical cells with current interrupt devices, J. Loss Prev. Process. Ind. 94 (2025) 105488.
[4] K.C. Abbott, J.E. Buston, J. Gill, S.L. Goddard, D. Howard, G. Howard, E. Read, R.C. Williams, Comprehensive gas analysis of a 21700 $Li(Ni_{0.8}Co_{0.1}Mn_{0.2})O_2$ cell using mass spectrometry, J. Power Sources 539 (2022) 231585.
[5] Committee on Toxicology and Board on Environmental Studies and Toxicology, Acute Exposure Guideline Levels for Selected Airborne Chemicals, Volume 4, The National Academies Press, Washington, DC, 2004.
[6] H. Li, Q. Duan, C. Zhao, Z. Huang, Q. Wang, Experimental investigation on the thermal runaway and its propagation in the large format battery module with $Li(Ni_{1/3}Co_{1/3}Mn_{1/3})O_2$ as cathode, J. Hazard Mater. 375 (2019) 241–254.
[7] H. Yang, G. Zhuang, P. Ross Jr., Thermal stability of $LiPF_6$ salt and Li-ion battery electrolytes containing $LiPF_6$, J. Power Sources 161 (2006) 573–579.
[8] T. Kawamura, S. Okada, J.-i. Yamaji, Decomposition reaction of $LiPF_6$-based electrolytes for lithium ion cells, J. Power Sources 156 (2006) 547–554.
[9] F. Larsson, P. Andersson, P. Blomqvist, A. Loren, B.-E. Mellaner, Characteristics of lithium-ion batteries during fire tests, J. Power Sources 271 (2014).
[10] F. Larsson, P. Andersson, P. Blomqvist, B.-E. Mellander, Toxic fluoride gas emissions from lithium-ion battery fires, Sci. Rep. 7 (1) (2017) 10018.
[11] P. Ribière, S. Grugeon, M. Morcrette, S. Boyanov, S. Laruelle, G. Marlair, Investigation on the fire-induced hazards of Li-ion battery cells by fire calorimetry, Energy Env. Sci. 5 (1) (2012).
[12] J. Jeevarajan, C. Lopez, S. Azam, S. Kinyon, Thermal runaway propagation testing study for safe transportation of lithium-ion cells and batteries, in: AIAA Propulsion and Energy 2019 Forum, Am. Inst. Aeronaut. Astronaut., Indianapolis, IN, 2019.
[13] C.I. Sanders, K.A. Oberlander, R.M. Spearrin, Polytetrafluoroethylene (PTFE) burn characteristics and toxicant formation in an oxidizer cross-flow via laser absorption tomography, PROCI 40 (2024) 105394.
[14] S. Koch, A. Fill, K.P. Birke, Comprehensive gas analysis on large scale automotive lithium-ion cells in thermal runaway, J. Power Sources 398 (2018) 106–112.
[15] R.K. Hanson, R.M. Spearrin, C.S. Goldenstein, Spectroscopy and Optical Diagnostics for Gases, Springer International Publishing, Cham, Switzerland, 2016.
[16] I.E. Gordon, L.S. Rothman, R.J. Hargreaves, R. Hashemi, et al., The HITRAN2020 molecular spetroscopc database, J. Quant. Spectrosc. Radiat. Transf. 277 (2022) 107949.
[17] K. Kar, S. Roberts, R. Stone, M. Oldfield, Instantaneous exhaust temperature measurements using thermocouple compensation techniques, in: SAE 2004 World Congress & Exhibitionm, Society of Automotive Engineers, Detroit, MI, 2004.
[18] S. Whitaker, Forced convection heat transfer correlations for flow in pipes, past flat plates, single cylinders, single spheres, and for flow in packed beds and tube bundles, AIChE J. 18 (1972) 361–371.
[19] A.P. Nair, D.D. Lee, D.I. Pineda, J. Kriesel, W.A. Hargus, J.W. Bennewitz, S.A. Danczyk, R.M. Spearrin, MHz laser absorption spectroscopy via diplexed RF modulation for pressure, temperature, and species in rotating detonation rocket flows, Appl. Phys. B 126 (138) (2020).

ATTACHMENT 2.

TOXIC FLUORIDE GAS EMISSIONS FROM LITHIUM-ION BATTERY FIRES BY FREDRIK LARSSON, PETRA ANDERSSON, PER BLOMQVIST, & BENGT-ERIK MELLANDER (LARSSON STUDY).

SCIENTIFIC REPORTS

Correction: Author Correction

OPEN

Toxic fluoride gas emissions from lithium-ion battery fires

Fredrik Larsson[1,2], Petra Andersson[2], Per Blomqvist[2] & Bengt-Erik Mellander[1]

Received: 11 April 2017
Accepted: 28 July 2017
Published online: 30 August 2017

Lithium-ion battery fires generate intense heat and considerable amounts of gas and smoke. Although the emission of toxic gases can be a larger threat than the heat, the knowledge of such emissions is limited. This paper presents quantitative measurements of heat release and fluoride gas emissions during battery fires for seven different types of commercial lithium-ion batteries. The results have been validated using two independent measurement techniques and show that large amounts of hydrogen fluoride (HF) may be generated, ranging between 20 and 200 mg/Wh of nominal battery energy capacity. In addition, 15–22 mg/Wh of another potentially toxic gas, phosphoryl fluoride (POF_3), was measured in some of the fire tests. Gas emissions when using water mist as extinguishing agent were also investigated. Fluoride gas emission can pose a serious toxic threat and the results are crucial findings for risk assessment and management, especially for large Li-ion battery packs.

Lithium-ion batteries are a technical and a commercial success enabling a number of applications from cellular phones to electric vehicles and large scale electrical energy storage plants. The occasional occurrences of battery fires have, however, caused some concern especially regarding the risk for spontaneous fires and the intense heat generated by such fires[1–5]. While the fire itself and the heat it generates may be a serious threat in many situations, the risks associated with gas and smoke emissions from malfunctioning lithium-ion batteries may in some circumstances be a larger threat, especially in confined environments where people are present, such as in an aircraft, a submarine, a mine shaft, a spacecraft or in a home equipped with a battery energy storage system. The gas emissions has however only been studied to a very limited extent.

An irreversible thermal event in a lithium-ion battery can be initiated in several ways, by spontaneous internal or external short-circuit, overcharging, external heating or fire, mechanical abuse etc. This may result in a thermal runaway caused by the exothermal reactions in the battery[6–10], eventually resulting in a fire and/or explosion. The consequences of such an event in a large Li-ion battery pack can be severe due to the risk for failure propagation[11–13]. The electrolyte in a lithium-ion battery is flammable and generally contains lithium hexafluorophosphate ($LiPF_6$) or other Li-salts containing fluorine. In the event of overheating the electrolyte will evaporate and eventually be vented out from the battery cells. The gases may or may not be ignited immediately. In case the emitted gas is not immediately ignited the risk for a gas explosion at a later stage may be imminent. Li-ion batteries release a various number of toxic substances[14–16] as well as e.g. CO (an asphyxiant gas) and CO_2 (induces anoxia) during heating and fire. At elevated temperature the fluorine content of the electrolyte and, to some extent, other parts of the battery such as the polyvinylidene fluoride (PVdF) binder in the electrodes, may form gases such as hydrogen fluoride HF, phosphorus pentafluoride (PF_5) and phosphoryl fluoride (POF_3). Compounds containing fluorine can also be present as e.g. flame retardants in electrolyte and/or separator[17], in additives and in the electrode materials, e.g. fluorophosphates[18,19], adding additional sources of fluorine.

The decomposition of $LiPF_6$ is promoted by the presence of water/humidity according to the following reactions[20,21];

$$LiPF_6 \rightarrow LiF + PF_5 \quad (1)$$

$$PF_5 + H_2O \rightarrow POF_3 + 2HF \quad (2)$$

$$LiPF_6 + H_2O \rightarrow LiF + POF_3 + 2HF \quad (3)$$

[1]Department of Physics, Chalmers University of Technology, Kemivagen 9, SE-41296, Gothenburg, Sweden. [2]Safety and Transport, RISE Research Institutes of Sweden, Brinellgatan 4, SE-50115, Boras, Sweden. Correspondence and requests for materials should be addressed to F.L. (email: vegan@chalmers.se)

Battery	Numbers of batteries per test	Type	Nominal capacity per battery (Ah)	Nominal voltage per battery (V)	Cell packaging
A	5–10	LCO ($LiCoO_2$)	6.8	3.75	Prismatic hard Al-can
B	2	LFP ($LiFePO_4$)	20	3.2	Pouch
C	5	LFP ($LiFePO_4$)	7	3.2	Pouch
D	9	LFP ($LiFePO_4$)	3.2	3.2	Cylindrical
E	5	LFP ($LiFePO_4$)	8	3.3	Cylindrical
F	2	NCA-LATP ($LiNiCoAlO_2$-$LiAlTiPO_4$)	30	2.3	Pouch
G	2	Laptop pack*	5.6	11.1	Cylindrical

Table 1. Details of the tested Li-ion battery cells. *Each laptop battery pack has 6 cells of type 18650; arranged 2 in parallel and 3 in series.

Of these PF_5 is rather short lived. The toxicity of HF and the derivate hydrofluoric acid is well known[22–24] while there is no toxicity data available for POF_3, which is a reactive intermediate[25] that will either react with other organic materials or with water finally generating HF. Judging from its chlorine analogy $POCl_3$/HCl[24], POF_3 may even be more toxic than HF. The decomposition of fluorine containing compounds is complex and many other toxic fluoride gases might also be emitted in these situations, however, this study focuses on analysis of HF and POF_3.

Although a number of qualitative and semi-quantitative attempts have been made in order to measure HF from Li-ion batteries under abuse conditions, most studies do not report time dependent rates or total amounts of HF and other fluorine containing gases for different battery types, battery chemistries and state-of-charge (SOC). In some measurements reported, HF has been found, within limited SOC-variations, during the abuse of Li-ion battery cells[15,16,26], as well as detected during the abuse of battery packs[27]. However, time-resolved quantitative HF gas emission measurements from complete Li-ion battery cells undergoing an abusive situation have until now only been studied to a limited extend; for a few SOC-values, including larger commercial cells[28,29], a smaller-size commercial cell[30] and a research cell (i.e. non-commercial cell)[31]. Time-resolved quantitative HF measurements on the gas release from complete electric vehicles including their Li-ion battery packs during an external fire have also been performed[32]. Other types of gas emissions from Li-ion cells during abuse have been the subject of a somewhat larger number of investigations[33–41]. Since the electrolyte typically is the primary source of fluorine, measurements of fluorine emissions from battery type electrolytes have been studied. For example, fire or external heating abuse tests have been performed on electrolytes[42–46] and the quantitative amounts of HF and POF_3 have been measured in some cases[45,46]. Other studies of electrolytes exposed to moderate temperatures, 50–85 °C, show the generation of various fluorine compounds[20,21,47–49] and some studies include both electrolyte and electrode material[50,51,52].

Our quantitative study of the emission gases from Li-ion battery fires covers a wide range of battery types. We found that commercial lithium-ion batteries can emit considerable amounts of HF during a fire and that the emission rates vary for different types of batteries and SOC levels. POF_3, on the other hand, was found only in one of the cell types and only at 0% SOC. The use of water mist as an extinguishing agent may promote the formation of unwanted gases as in eqs (2)–(3) and our limited measurements show an increase of HF production rate during the application of water mist, however, no significant difference in the total amount of HF formed with or without the use of water mist.

Lithium-ion battery fire tests. The experiments were performed using an external propane burner for the purpose of heating and igniting the battery cells as described in the Methods section. Seven different types of batteries, type A-G, were investigated, from seven manufacturers and with different capacity, packaging type, design and cell chemistry, as specified in Table 1. Type A had a lithium cobalt oxide (LCO) cathode and carbon anode, types B to E had lithium-iron phosphate (LFP) cathode and carbon anode, type F had nickel cobalt aluminum oxide (NCA) and lithium aluminum titanium phosphate (LATP) electrodes while type G was a laptop battery pack with unspecified battery chemistry. All electrolytes contained $LiPF_6$. Most of the cells were tested for different SOC levels, from fully charged, 100% SOC, to fully discharged, 0% SOC. The study included large-sized automotive-classed cells, i.e. series production cells of high industry quality, with long life time etc.

The heat release rate (HRR) and the emitted HF for B-type cells with different SOC values are shown in Fig. 1. Only the 100% SOC cells show several distinct peaks, corresponding to intense flares, when the cells vented and the emitted gas burn, for all other cells the heat release as a function of time is more smooth. These behaviors are reproducible also for the other tested cell types, e.g., only the 100% SOC cells show the more violent heat release peaks with intense flares.

The measurements of the gas emissions during the fire tests show that the production of HF is correlated to the increase in HRR although somewhat delayed. From Fig. 1b it is evident that the higher SOC value, the higher values for the peak HF release rate. The total amount of HF varies considerably for the different battery types, see Fig. 2a. The amount of HF produced, expressed in mg/Wh, where Wh is the nominal battery energy capacity, is approximately 10 times higher for the cell with the highest values compared to the cells with the lowest values. The different relative amount of electrolyte and filler materials in the cells could be the simple explanation of this variation but information on those amounts are difficult to access for commercial batteries. The highest HF values are found for the pouch cells, a possible explanation would be that hard prismatic and cylindrical cells can build a

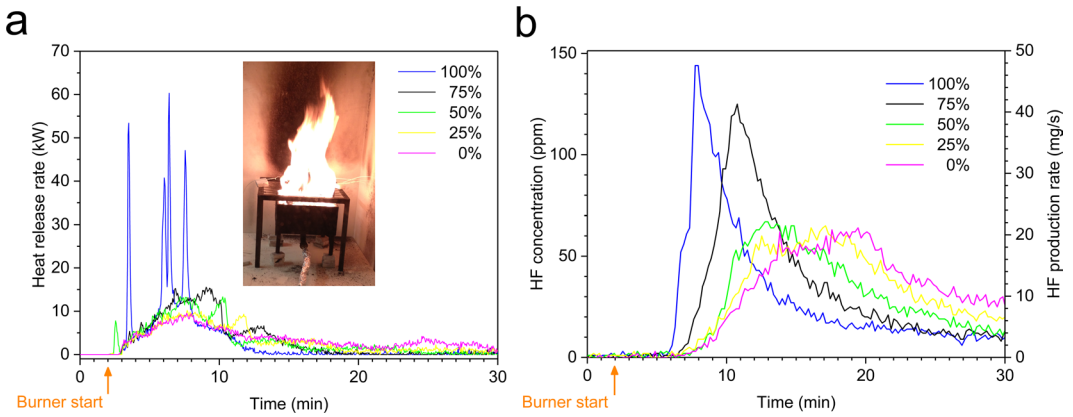

Figure 1. Results for type B cells, for 0–100% SOC with intermediate SOC-steps of 25%, exposed to an external propane fire; (**a**) showing the heat release rate (burner HRR contribution is subtracted), the inset photo shows burning battery cells during the test; (**b**) showing the HF release both as the measured concentrations as well as the calculated HF production rates. The HF production rates are calculated from the measured HF concentration by the Ideal gas law taking into account the ventilation flow, see Methods. The starting time of the heating process is marked on the time axis.

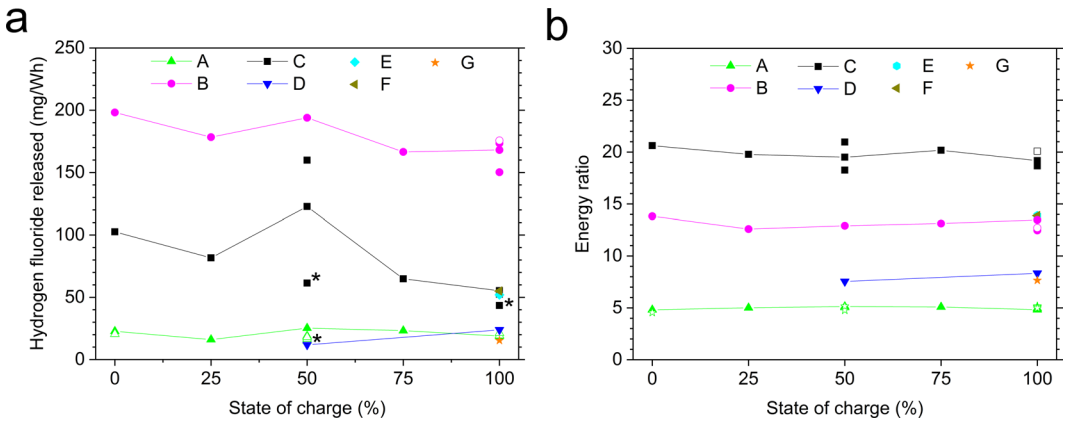

Figure 2. Total amount of HF measured by FTIR, normalized to nominal electrical energy capacity (**a**) and the energy ratio (**b**), for seven types of Li-ion battery cells and with various state of charge levels. Non-filled symbols indicate a repetition variant, e.g. applying water mist. The lines are intended as a guide for the eye. The energy ratio is a dimensionless value calculated by taking the total heat release from the battery fire divided by the nominal electrical energy capacity. Note that for 100% SOC the values are overlapping for type C, E and F as well as for type A, D and G in (**a**) and type B, E and F in (**b**). *Low value for type C at 50% and 100% SOC and type D at 50% SOC due to that a pre HF-saturation was not applied, therefore a part of the HF release was likely to be saturated in the gas sampling system, see Methods.

higher pressure before bursting, rapidly releasing a high amount of gases/vapors from the electrolyte. Due to the high velocity of the release and thus the short reaction time, combustion reactions might be incomplete and less reaction products might be produced. In the test involving type G the cylindrical cells were layered horizontally, thus having a different venting direction and possibly increased wall losses, which combined with a very energetic response, might suggest why HF was detected only from the filter analysis and not detected by FTIR-analysis. The tested pouch cells of type B and C burned for longer time and with less intensity. The pouch cell of type F, however, burned faster, possibly due to its different electrode materials. The SOC influence on the HF release was less significant and the trend in Fig. 2a shows higher HF values for 0% than for 100% SOC, however with clear peaks at 50% SOC. Although these results are reproducible, they are difficult to explain. In other studies[30,31], significantly narrower in test scope, involving smaller-sized cells and using a somewhat different abuse method, it was found that the total amount of HF measured by real-time FTIR was higher for decreasing SOC (tests conducted at 100%, 50% and 0% SOC).

The HRR curve is used to calculate the total heat release (THR) which corresponds to the energy released from the burning battery. THR is obtained by integrating the measured HRR (with the burner contribution subtracted) over the complete test time. Fig. 2b shows the energy ratio, that is how much energy is produced by the burning

Battery	Nominal energy capacity (Wh)	Normalized total HF detected with FTIR (mg/Wh)	Normalized maximum HRR (W/Wh)	Normalized THR (kJ/Wh)
A	128	15–25	243–729	17–19
B	128	150–198	78–633	45–50
C	112	43–160	116–491	66–75
D	92	12–24	207–315	27–30
E	132	52	235	50
F	138	55	384	50
G	124	15	460	28

Table 2. Main test results normalized to nominal energy capacity, when applicable including various SOC-levels.

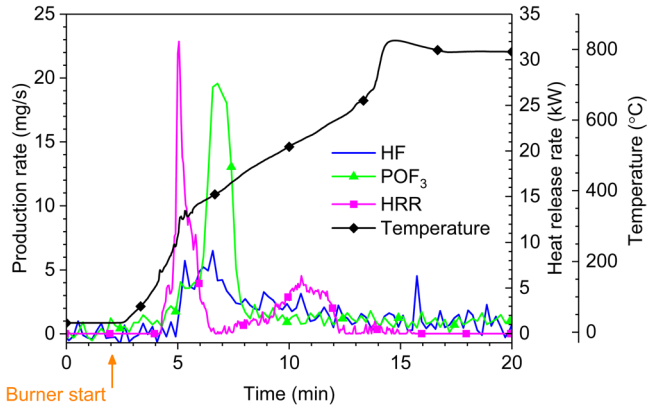

Figure 3. Results for a test with 5 type A cells at 0% SOC showing HF and POF_3, HRR and average surface temperature of the battery cells.

battery, compared to the amount of nominal electrical energy capacity a fully charged battery can deliver to an external circuit. The energy ratio is therefore a comparison between the chemical and the electrical energy of the Li-ion battery cell. The energy ratio varies considerably for the different cell types but is approximately constant for each cell, independent of SOC level. There are some similarities in Fig. 2a and b for the pouch cells, type B and C, which give the highest values in both cases, although in reverse order. This might indicate a higher amount of combustibles, e.g. electrolyte, in these cells compared to the other cells. It is also interesting to see that the energy ratio varies significantly between the tested cells, ranging from 5 to 21. This is important knowledge for fire protection and fire fighting. The energy ratio thus refers to a nominal fully charged battery while in normal use only a part of the SOC-window is used, for example half (50%) of the SOC-window (corresponding to cycling the battery between e.g. 30% and 80% SOC). If instead, the total heat release divided by the used electric battery capacity in the specific application is considered, higher energy ratio values are obtained. A summary of the results is shown in Table 2.

The measured heat release from an overheated battery may include several aspects, e.g. the battery temperature increase and the combustion of released gases. Variations due to the type of battery cell, the initiation method, e.g. if the test is done as an external fire test, an external heating or an overcharge test, and the test method, e.g. access to ambient oxygen (inert, under-ventilated or well-ventilated fire), and the presence of an external igniter, can greatly affect the amount of measured heat release. Energy release from a internal cell event in a confined environment can, for example, be lower than the energy release from the same cell in case of external fire. Thus energy ratios published using other methods and other types of Li-ion cells can be significantly different[7,52,53].

For all tested battert types and selected SOC-levels, POF_3 could only be measured quantitatively for type A battery cells at 0% SOC. Repeated measurements confirmed the presence of POF_3 only for type A and only for 0% SOC. No POF_3 could thus be detected in any of the other tests. POF_3 is an intermediate compound and the local combustion conditions in every test, will influence the amounts of POF_3 generated. This shows the importance of investigating many different set-ups when evaluating emitted gases.

In Fig. 3 the HRR, the average surface temperature of the five cells as well as the HF and POF_3 production rates are shown for type A cells at 0% SOC. The POF_3 curve is less noisy than the HF curve due to different signal-to-noise ratios of the FTIR instrumentation at the different wavenumbers. There is a secondary peak in HRR approximately 5 minutes after the main heat event, this peak does not correspond to any peaks in the mass flow of HF or POF_3. The explanation for this could be that the second peak in the heat release rate involves burning of mainly non-fluorine containing compounds. The temperature curve shows a rapid increase above the

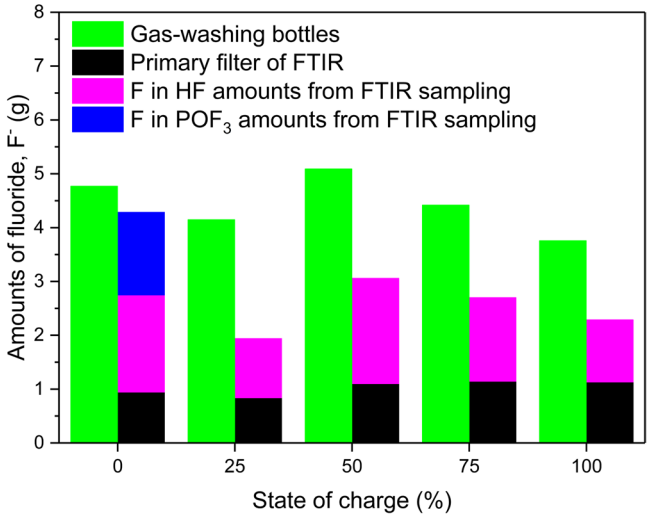

Figure 4. Total amount of measured fluoride, F^-, for type A, for 0–100% SOC with intermediate steps of 25%. The amount of F^- from the FTIR is calculated from the measurement results for POF_3 and HF, while the amount of fluoride from gas-washing bottles and primary filter analyses is measured as water soluble fluoride.

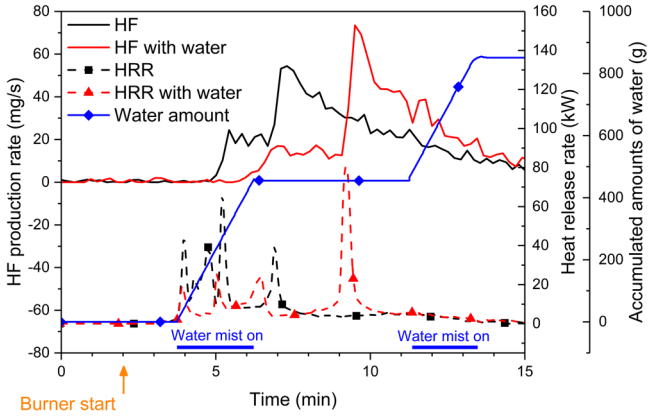

Figure 5. Results for type B cells at 100% SOC with and without the use of water mist.

melting temperature of the alumina cell case at about 660 °C. At these temperatures the alumina is molten and has formed a puddle on the burner bed beneath the battery cells. The thermal conditions in and around the thermocouples and the remains of the batteries have therefore changed considerably causing the apparent temperature increase.

In addition to the time resolved measurements with the FTIR, gas-washing bottles were used to determine the total fluorine content in the gas emissions during the tests. A comparison between the different measurement methods used can be seen in Fig. 4 for type A cells. Note that the FTIR measurements are performed only to detect HF and POF_3, other fluoride compounds are not included. It is interesting to note that for 0% SOC the total amount of fluoride measured by the gas-washing bottle technique matches rather well with the FTIR and primary filter analysis. For other SOC values the fluoride content is higher from the gas-washing bottle measurements. Still, the general trend observed in the FTIR measurements for different SOC values is more or less confirmed by the gas-washing bottle measurements.

Gas-washing bottles were also used for some of the tests involving battery types B and C. These batteries showed higher amounts of released HF compared to type A. The ratio between the total values of released flouride from FTIR plus filter analysis and from the gas-washing bottles for type B and C was between 0.89 and 1.02, indicating a better correlation between FTIR and gas-washing bottles measurement when HF gas emissions are higher.

The total amount of POF_3 measured by FTIR for type A at 0% SOC was 2.8 g (for 5-cells) and 3.9 g (for 10 cells). Hence, the normalized total POF_3 production was 15–22 mg/Wh of nominal battery energy capacity. Abuse studies measuring POF_3 are few, Andersson *et al.*[46] found both HF and POF_3 when burning mixtures of propane and Li-ion battery electrolytes with a HF:POF_3 production ratio between 8:1 and 53:1. Besides HF and POF_3 measurements, several distinct non-assigned peaks were found in the FTIR measurements, e.g. at 1027 cm^{-1}

Battery	SOC (%)	Number of tests	Normalized total HF detected (mg/Wh)		Normalized maximum HRR (W/Wh)	Normalized THR (kJ/Wh)
			From FTIR	From gas-washing bottles		
A	100	6	19.8 ± 1.2 [3]	29.1 ± 3.1 [5]	612 ± 102	18.1 ± 0.46
	50	7	18.5 ± 3.9 [6]	36.7 ± 3.3 [6]	416 ± 39 [6]	18.0 ± 0.61 [6]
	0	2	21.6 ± 1.5	38.3 ± 1.6	214 ± 53	16.8 ± 0.66
B	100	4	166.8 ± 11.5	191.3 ± 11.3 [2]	538 ± 77	46.9 ± 1.9
C	100	3	53.9 ± 2.0 [2]*	N/A	461 ± 27	69.5 ± 2.6
	50	3	141.3 ± 26.3 [2]*	N/A	149 ± 5	70.5 ± 4.9

Table 3. Detailed results for all available repetitions. Values presented as mean values followed by the standard deviation, in case the data parameter was not measured in all tests the value in bracket declares the number of available tests used for the specific data parameter value. *For FTIR data for battery type C, one data point of 50% and one data point at 100% SOC are excluded as outliers since they were low due to that a pre HF-saturation was not applied in the test, see Methods.

and 1034 cm^{-1}, which have also been seen in other studies[46]. They are compatible with the typical C-O stretching energies of low molecular weight alcohols in gas phase but also with in-plane stretching of aromatic compounds. This indicates the complexity and the limited knowledge in this area.

Water mist measurements. In order to study the effects of water on gas emissions, fire tests have also been performed where a water mist was applied during the fire. The reason for this experiment is that water is the preferred extinguishing agent for a lithium-ion battery fire. The intention in this study was however not to extinguish the fire completely. One potential problem regarding the use of water mist is that the addition of water may, in principle, increase the rate of formation of HF, see Eqs (2) and (3).

Figure 5 shows the results for type B cells with and without exposure to water mist, note that both the HRR and HF production are delayed when water mist is used. In this limited study, the peak of the HF production rate increased by 35% when using water, however no significant change in the total amounts of the HF release could be seen. A similar result has been reported in a previous study[28]. The water mist was applied during two different periods of time, as marked in Fig. 5, adding a total of 851 g of water in the reaction zone, however, several other large sources of water were also present in the experiment, i.e. water production from the propane combustion and from humidity in the air. The water mist is cooling the fire and the top surface of the pouch cell was for some time partly covered with liquid water; this is the reason that the battery fire is delayed as seen in Fig. 5. The water mist might actually also clean the air by collecting fume particles and HF can be bound to water droplets, thus possibly lowering the amount of HF in the smoke duct and increasing the non-measured amount of very toxic hydrofluoric acid on the test area surfaces (e.g. walls, floor, smoke duct walls).

Repeatability

Repeated tests were performed for battery types A-C for selected SOC-levels. Some of the repetitions included a variant, e.g. including water mist; see Methods. In Fig. 2 all available test data are presented. Since the test repetitions are not clearly observable in Fig. 2 the results are also presented in Table 3 showing the mean values and standard deviations and the number of performed tests. While the ranges in Table 2 include data for all tested SOC-values, Table 3 shows test data for repeated measurements including repetition variants.

Figure 6 shows the repeatability results for four tests of battery type B for 100% SOC. The time evolution of HRR varies in the fire tests as seen in Fig. 6a. In fire tests there are always natural variations, however comparing the tests with 100% SOC, in Fig. 6a, with those with lower SOC-values presented in Fig. 1a, the repeatability of the 100% SOC tests is significant. The third repetition (black line) in Fig. 6a is delayed due to that it included an application of water mist, as discussed above. Although the appearance of the HRR plots of the four tests differs in Fig. 6a the THR (the integrated HRR) values are rather similar. Fig. 6b shows the HF release for the same four tests of type B at 100% SOC. Repetition 2 and 3 were performed in the third test period, without secondary FTIR filter, and therefore Repetition 2 occurs earlier while Repetition 3 is delayed due to the applied water mist, as discussed above. For the four tests of type B at 100% SOC the mean value of the total FTIR detected HF release is 166.8 mg/Wh with a standard deviation of 11.5 mg/Wh, as seen in Table 3. Comparing Fig. 1b and Fig. 6b, shows that for 100% SOC the HF release is faster and reaches a higher value. Repetition 1 in Fig. 6b shows lower HF release peak values, however, the total HF release value from the FTIR measurement of 168 mg/Wh is close to the average value (166.8 mg/Wh, as seen in Table 3).

Conclusions

This study covered a broad range of commercial Li-ion battery cells with different chemistry, cell design and size and included large-sized automotive-classed cells, undergoing fire tests. The method was successful in evaluating fluoride gas emissions for a large variety of battery types and for various test setups.

Significant amounts of HF, ranging between 20 and 200 mg/Wh of nominal battery energy capacity, were detected from the burning Li-ion batteries. The measured HF levels, verified using two independent measurement methods, indicate that HF can pose a serious toxic threat, especially for large Li-ion batteries and in confined environments. The amounts of HF released from burning Li-ion batteries are presented as mg/Wh. If extrapolated for large battery packs the amounts would be 2–20 kg for a 100 kWh battery system, e.g. an electric

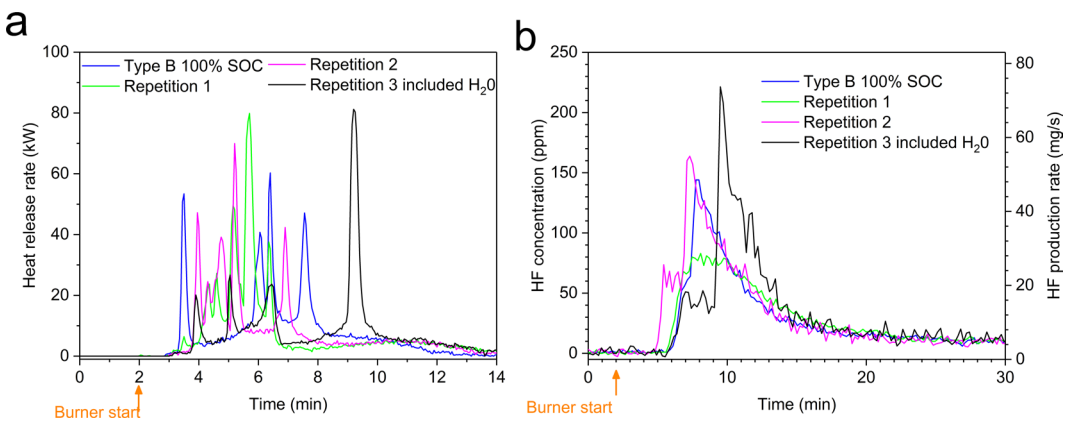

Figure 6. Repeatability for four tests of type B cells at 100% SOC, (**a**) shows the heat release rate (burner HRR contribution is subtracted) and (**b**) shows the HF release, both as the measured concentrations as well as the calculated HF production rates.

vehicle and 20–200 kg for a 1000 kWh battery system, e.g. a small stationary energy storage. The immediate dangerous to life or health (IDLH) level for HF is 0.025 g/m^3 (30 ppm)[22] and the lethal 10 minutes HF toxicity value (AEGL-3) is 0.0139 g/m^3 (170 ppm)[23]. The release of hydrogen fluoride from a Li-ion battery fire can therefore be a severe risk and an even greater risk in confined or semi-confined spaces.

This is the first paper to report measurements of POF_3, 15–22 mg/Wh, from commercial Li-ion battery cells undergoing abuse. However, we could only detect POF_3 for one of the battery types and only at 0% SOC, showing the complexity of the parameters influencing the gas emission. No POF_3 could be detected in any of the other tests.

Using water mist resulted in a temporarily increased production rate of HF but the application of water mist had no significant effect on the total amount of released HF.

The research area of Li-ion battery toxic gas emissions needs considerable more attention. Results as those presented here are crucial to be able to conduct a risk assessment that takes toxic HF gas into account. The results also enable strategies to be investigated for counteractions and safety handling, in order to achieve a high safety level for Li-ion battery applications. Today we have a rapid technology and market introduction of large Li-ion batteries but the risks associated with gas emissions have this far not been possible to take into consideration due to the lack of data.

Methods

Seven types of Li-ion batteries were exposed to an external propane fire. Fire characteristics, gas emissions, battery temperatures and cell voltages were measured. In total 39 fire tests were conducted of which 20 were within the base test matrix, 19 were repeated measurements of selected battery types and SOC-levels of which 10 included a variant, e.g. water mist for fire-fighting. The amounts of emitted fluoride gases were measured with two parallel and independent techniques, FTIR (time resolved concentration measurements and total values achieved by integration of the time resolved curve) and gas-washing bottles (total values). The experimental setup is schematically shown in Fig. 7. The gas collecting system and measurement system of the *Single Burning Item (SBI) method* (EN 13823[54]), which is normally used for reaction-to-fire classification of construction products according to EN 13501-1[55] was used in the tests. The tests were performed in three different test periods; the second test period was conducted about 1 year after the first and the third test period was conducted about 2.5 years after the first. Each test period involved several days of testing. The measurement equipment, as specified in the text below, was somewhat varying between the three test periods.

Batteries. Six different types of Li-ion battery cells, type A-F, and one Li-ion battery pack, type G, were tested as seen in Table 1. The number of cells used in each test was varied in order to achieve similar electrical energy capacity per test. The batteries were placed on wire gratings just above a 16 kW propane burner. The wire grating was made of steel wire about 2 mm thick over a surface of about 300 × 300 mm. The quadrants of the grating were 40 × 100 mm. The cells were not electrically connected to each other (except the laptop packs of type G, see note in Table 1). Type A-F was pure battery cells while type G was a complete laptop battery pack which included plastics box, electronics and cables. The chemical content of the polymer materials in the auxiliary components of the battery pack of battery type G is not known. It is possible, however not likely, that fluorine was included in some of the components, which in that case could have resulted in the production of HF. For battery type A, 5 cells/test was used except in two variant tests in which 10 cells/test were used.

The influence of different state of charge was investigated, for some battery types the complete SOC-window ranging from 0% to 100%, with intermediate steps of 25%, was investigated. The SOC levels included for each battery type and the numbers of repetitions per test type, i.e. the fire test matrix, is seen in Table 4. All parameters were not measured in all of the tests. Measurement of HRR and corresponding THR was conducted in 38 tests, FTIR in 35 tests and gas-washing bottles were used in 19 tests.

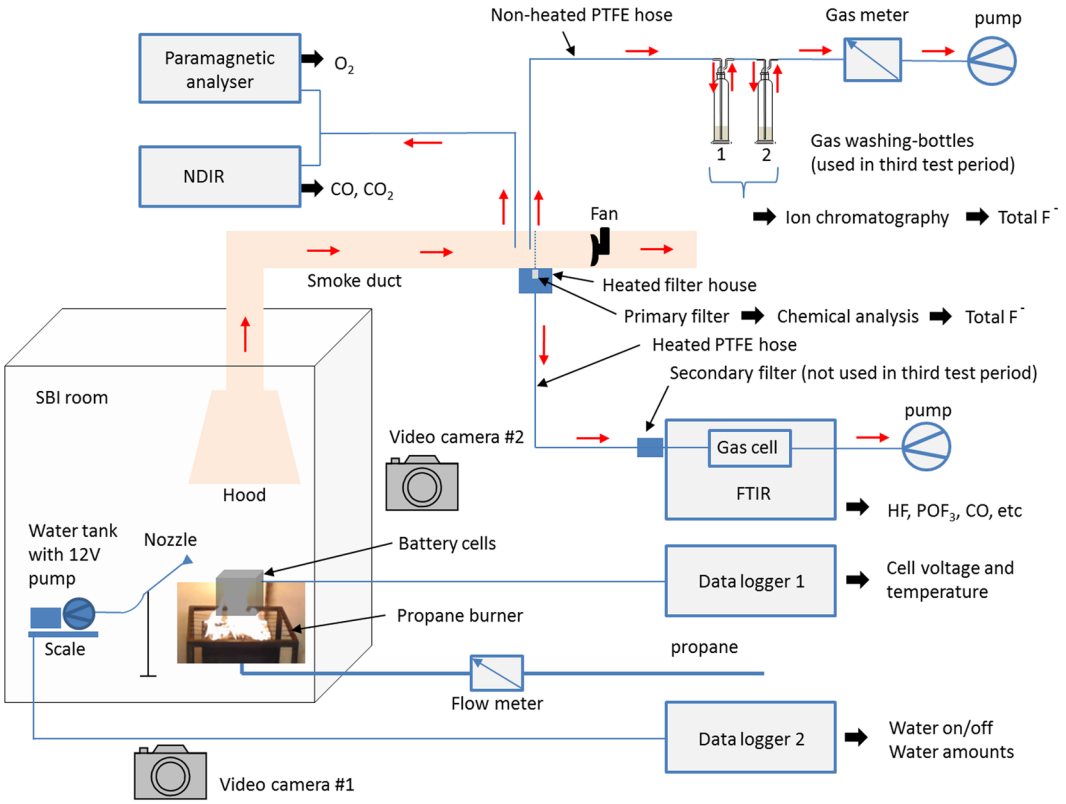

Figure 7. Schematic illustration of the experimental setup.

Battery	Number of tests per SOC-level					Number of tests
	0%	25%	50%	75%	100%	
A	1 + 1*	1	3 + 4*	1	3 + 3*	17
B	1	1	1	1	3 + 1*	8
C	1	1	3	1	2 + 1*	9
D			1		1	2
E					1	1
F					1	1
G					1	1
Total number of tests						39

Table 4. Detailed test matrix of the fire tests. *repetition includes a variant, e.g. water mist or 2 × 5-cell-pack (for battery type A).

The selected SOC level in each test was set using a charge/discharge procedure using ordinary laboratory equipment as well as dedicated battery test equipment, i.e. a *Digatron battery tester* and *Metrohm Autolab PGSTAT302N* with 20 A booster module. The cells were first fully charged by constant current followed by constant voltage (CC-CV) according to the manufacturer's instructions. For cells intended for tests with less than 100% SOC, the cell was discharged to the selected SOC level, using constant discharge current (CC). A relative low current rate, about C/5, was used and voltage and current rates were within the manufacturer limits. In most cases each battery type was tested during the same test period. However, the tests for type C and D were split in several test periods, for type C repetitions on 50% SOC were conducted in all three test periods, and for type B repetitions at 100% SOC were made in two test periods, the latter one included a water mist test.

All batteries were unused and the calendar life time of the cells before the tests were approximately 6–12 months for type A, F and G and between approximately 2–3 years for type B-E. The pouch cells; type B, C and F was mechanically tied together with steel wires (0.8 mm diameter). The type A hard prismatic cells were tight together in packs of five cells, "5-cell-pack", using steel straps (1 × 13 mm). The hard prismatic and cylindrical cells were placed in boxes to protect test personnel from potential projectile hazards in case of cell explosions due to excessive pressure. The 5-cell-pack of type A was placed standing up, with the cell safety vents releasing straight upright in direction to the hood and smoke duct, inside a custom-made steel-net-box, see Fig. 8. Additionally, the 5-cell-pack of type A was fastened to the bottom of the steel-net-box with steel wire (0.8 mm diameter) in the

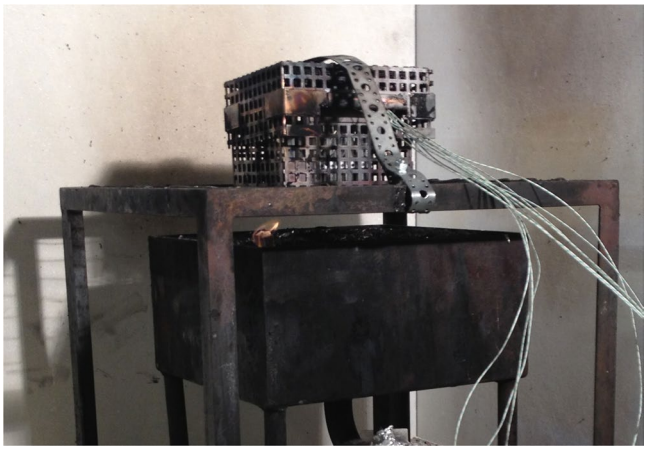

Figure 8. Photo of test type A, showing the 5-cell-pack inside a steel-net-box placed on the wire gratings. The sand bed for the propane burner is underneath the wire grating, a pilot flame (seen in front left corner of the burner) is used to ignite the propane gas.

corners to avoid it moving around due to e.g. explosion/rupture/venting. Type D and E cells were placed standing up in custom-made boxes made of non-combustible silica board and steel net at the top and bottom. Type G was placed in a steel net. The protective boxes and steel net were fastened in the wire gratings with steel wire and steel straps to avoid movement due to response to the fire. Care was taken to avoid external short circuiting when placing the battery on the wire gratings as well as avoiding accidental external electrical inter-cell-connections, e.g. for pouch cells the electrical tab terminals were cut. Still the battery test setup allowed that the separators and electrical insulation in the cells could melt due to the heat exposure which could cause various internal and external electrical contacts.

The battery surface temperature was measured with several type K thermocouples; the number of sensors varied for the different battery types. Battery cell surface temperature values presented in this paper are average values over the cell. Cell voltages were measured for type A, B, C and F battery tests. Cell voltage and thermocouple readings was sampled with 1 Hz using two types of data loggers, *Agilent 34972 A using an Agilent 34902 A reed multiplexer module* (for the third test period) and *Pico Technology ADC-24* (for the first and second test period).

Test procedure. The propane burner was started 2 minutes into each test, as indicated with arrows in the result figures in the paper. The burner was active as long as there was a heat contribution from the burning batteries; therefore, the burner was active for different durations of time for different batteries and SOC-levels. When the heat release from the batteries was no longer detectable, the power of the propane burner was doubled, i.e. to 32 kW, in order to be sure to fully burn out any residues of the batteries, for increased personnel safety. The fire emissions were collected in the hood and transferred in the smoke duct having a ventilation flow of 0.4 m^3/s, with the exception that 0.6 m^3/s was used in two tests with 100% SOC for type C. For these cases the values were scaled down to the lower flow values making the results from the two flow rates comparable. The SBI-room, see Fig. 7, had a ventilation inlet from an adjacent indoor laboratory hall (which had fresh air inlet from the ventilation system in the building), supplying ambient air with temperature about 20 °C entering beneath the propane burner. We consider the amount of ambient air to be sufficient to provide an oxygen-rich environment and thereby consider the battery fire as well-ventilated. However for some tests, during the rapid and energetic gas outbursts, a full combustion might not have occurred in these short time periods.

All tests were video recorded and for the majority of the tests an additional camera was used set at 90 degree angle from the other video camera, allowing simultaneous recording from two sides of the battery fire.

A part of the smoke duct flow was sampled to a *Servomex 4100 Gas purity analyser* where the oxygen content was measured by a *paramagnetic analyser* and CO and CO_2 were measured by a *non-dispersive infrared sensor (NDIR)*. By combing these two measurements, the heat release rate (HRR) is calculated using the oxygen consumption method corrected by CO_2[54]. Each test day started with a blank test, i.e. using only the propane burner, to measure the HRR of the burner alone and measure blanks for FTIR and gas-washing bottles. In the presented HRR values of the battery tests the burner contribution to the HRR (about 16 kW, with slight daily variations, established by the blank tests) has been subtracted. The combined expanded uncertainty is ±5 kW for the HRR-values. By integrating the HRR values over the entire test, subtracting the HRR from the burner, the total heat release (THR) from the battery cells could be established. The oxygen consumption method is common in fire calorimetry, however when using it with batteries, the joule heating from electrical discharge within the cells is not accounted for, therefore the values of HRR and THR do not include the Joule heating. During the external fire tests, it is difficult to measure how much a battery cell is electrically discharged when the separator is melting. The energy ratios presented in Fig. 2b do not include any Joule heating as clearly stated by its definition. For 0% SOC the influence from Joule heating is in principle zero, however small amounts of joule heating might possibly be liberated when going to zero voltage even though other processes might occur. Li-ion cells can also release oxygen during thermal runaway and this could affect the measured O_2 levels. The amount of oxygen release varies

Spectral bands (cm^{-1})	Type of band
POF_3	
868–874	P-F symmetric stretching mode[20]
1413–1418	P-O stretching mode[20]
HF	
4172–4175	HF R-branch stretching mode[58]
4202–4203	HF R-branch stretching mode[58]

Table 5. FTIR spectral band used for measurements of POF_3 and HF.

for different electrode materials, e.g. LFP typically releases less oxygen than LCO. However, the ventilation flow is large and the O_2 released from the battery cells is regarded as negligible.

Gas measurements. Besides the gas measurements in the SBI apparatus, measurements of gases were also conducted by online Fourier transform infrared spectroscopy (FTIR). The FTIR offers broad and diverse spectra of gases, the focus was however on fluoride gas emissions. The FTIR used was a *Thermo Scientific Antaris IGS analyzer (Nicolet)* with a gas cell. The gas cell was heated to 180 °C and had a volume of 0.2 L, 2.0 m path length and a cell pressure of 86.7 kPa which was maintained during the tests. The spectral resolution of the FTIR was 0.5 cm^{-1} (accuracy 0.01 cm^{-1}) and 10 scans where used to collect a spectrum every 12 s, giving both accurate intensity, as well as relatively rapid measurements with its five spectrum per minute rate. A part of the duct flow, taken along the full duct pipe width (in the mid height of the pipe) from around 15 sampling holes (about 2 mm diameter, directed opposite to flow, pipe end was closed), was taken to online FTIR measurement. This sub-flow was extracted through a primary filter inside a heated filter house (180 °C) and then extracted through an 8.5 m sampling PTFE hose, heated to 180 °C, and then through a secondary filter and finally through the gas cell of the FTIR. The sub-flow was selected to be 3.5 L/min using a pump located after the FTIR gas cell. Between each test the FTIR sampling system was flushed with N_2 gas and a new background spectrum was measured. There is a natural delay time between the FTIR and the heat release measurement. In order to time synchronize them the (CO_2 measurements from both the FTIR and the NDIR) part of the heat release rate measurement, were overlayed.

One primary filter (M&C ceramic filter, type "F-2K") was used per test and was chemically analysed for fluoride content after the test. It is known that HF may be partly adsorbed by this type of filter[56]. The fluoride amount absorbed by the filter was determined by leaching the filter in an ultrasonic water bath for at least 10 min and thereafter the fluoride content in the water was measured by ion chromatography with a conductive detector, according to the method B.1 (b) of the SS-ISO 19702:2006 Annex B standard. The amount of HF is calculated by assuming that all fluoride ions present in the filter derives from HF. The secondary filter (M&C sintered steel filter), heated to 180 °C, was the same in all tests in the first and second test period. In the third test period the secondary filter was removed in order to decrease delay time and losses. The third test period started with burning 10 cells of type A in order to saturate the FTIR sampling system with HF and it was conducted because in the first and the second test period the first tests had indicated low HF values, HF was potentially lost during saturation of the gas collecting system.

The FTIR was calibrated[29,57] for HF and POF_3. The minimum detection limit (MDL) for HF was 1.7 ppm and the limit of quantification (LOQ) was established to 5.7 ppm. The detection limit for POF_3 was 6 ppm[29]. PF_5 was also qualitatively detectable by the FTIR[29] but not quantitatively calibrated. A classical least square (CLS) method was used for the quantification of HF and POF_3 using the spectral bands specified in Table 5. The relative error of the HF prediction is lower than 10 rel-%.

For all measurements, except type G, the measured ppm levels of HF were above the detection level. For POF_3, the maximum concentration was 11 ppm (5-cells) and 19 ppm (10-cells).

When the FTIR measurement stopped, HF levels were, in some of the tests, still somewhat above the detection limit, even though no HRR contribution was measured from the batteries. It is also possible that the HF was temporarily clogged in the sampling system. Some HF might not have been collected in the measurements and the effect of this error is largest for the batteries that give the lowest values. Thus the reported values might underestimate the released gas emissions.

In order to further improve the accuracy of the FTIR measurements, a data offset determination and a subsequent adjustment of the HF values was performed. The improvement was greatest for tests with lower concentrations, closer to the MDL value, e.g. type A with 5 cells with low values during relatively short periods of time. With 10 cells per test, the type A batteries gave higher signal-to-noise levels. The FTIR measurements started around 8 minutes before the burner was started. The calculated average HF ppm noise level was treated as an offset that had both negative and positive values, ranging from extreme values of about −2 to 3.5 ppm. This offset was compensated for by assuming a constant offset value and adding positive or negative offset values to the total HF release value. Note that the reported concentration values in ppm are only valid for the measurements in the smoke duct of our specific test equipment and method. The HF and POF_3 concentration values (in ppm) were used for calculating the corresponding production rates (in mg/s) using the ideal gas law and taking into account the measured ventilation flow rate in the smoke duct.

In the third test period the total amounts of water soluble fluorides were determined using gas-washing bottle technique. This was made in order to validate the results from the FTIR measurements with a separate measurement technique. The water soluble fluorides were collected in the bottles and the amount of HF was calculated by assuming that all fluoride ions present derives from HF. The sample gas was extracted from the center of

the smoke duct using a non-heated 6 mm (o.d.) diameter PTFE sampling tube with a length of about 1.5 m. The sampling was made using two gas-washing bottles connected in series each containing 40 mL of an alkaline buffer solution (20 mM Na_2CO_3/20 mM $NaHCO_3$). The second bottle was used to capture any losses from the first bottle. The sampling flow was 1.0 normal-L/min and the total sampled volume during a test was measured by a calibrated gas volume meter. The sampling flow rate was checked before the start of each test using a *Gilian Gilibrator-2 NIOSH Primary Standard Air Flow Calibrator* gas flow meter. The procedure during a test was to continuously sample during the full test time. When the test was completed, the sampling tube was disconnected from the exhaust duct to allow rinsing of the tube with buffer solution, about 30 mL in the first gas-washing bottle, to collect any fluoride deposited on the inner walls of the tubing, in order to minimize losses in the tube. Since the tube was rinsed, heating of the tube was not necessary (any condensation in tube was collected anyhow). Analysis of fluorine content of the absorption solutions was made using High Performance Ion Chromatography (HPIC). The contents of the two gas-washing bottles were analyzed separately. The bottles were rinsed with distilled water between each test in order to minimize any interference between tests.

Water mist test. In the water mist tests, a custom-made equipment was constructed, including a 12 V automotive pump and water container which was placed on a scale measuring the weight of the water. The scale readings and the on/off manual switching (of the 12 V) was recorded with 1 Hz using *Pico Technology ADC-24* with a custom-made *LabVIEW* program. The water mist was sprayed on or above the batteries using a metal nozzle. In order for precise time synchronization, the on/off 12 V signal was recorded by both data loggers (data logger 1 and data logger 2). A blank test, i.e. using only the propane burner and without batteries, was performed in order to calibrate the setup. The water flow was around 190 g water per min and consisted of deionized water.

References

1. Samsung Note 7: Press Conference Details, Samsung US, Our safety promise, http://www.samsung.com/us/explore/committed-to-quality/?CID=van-brd-brd-0119-10000141, Date of access: 06/04/2017.
2. Prigg, M. Nasa reveals shocking video of secretive military 'RoboSimian' EXPLODING as its batteries catch fire (2016), http://www.dailymail.co.uk/sciencetech/article-3883158/Nasa-reveals-shocking-video-secretive-military-RoboSimian-EXPLODING-batteries-catch-fire.html, Date of access: 06/04/2017.
3. Aircraft Serious Incident Investigation Report, JA804A. Japan Transport Safety Board (2014), Available online: http://www.mlit.go.jp/jtsb/eng-air_report/JA804A.pdf, Date of access: 13/02/2017.
4. Auxiliary Power Unit Battery Fire, Japan Airlines Boeing 787–8, JA829J, Boston, Massachusetts; NTSB/AIR-14/01. National Transportation Safety Board (2014), Available online: http://www.ntsb.gov/investigations/AccidentReports/Reports/AIR1401.pdf, Date of access: 13/02/2017.
5. Chevrolet Volt battery incident overview report, *National Highway Traffic Safety Administration (NHTSA)*, DOT HS 811 573 (2012).
6. Doughty, D. & Roth, E. P. A general discussion of Li ion battery safety. *The Electrochem. Soc. Interface*, **summer 2012**, 37–44 (2012).
7. Larsson, F. & Mellander, B.-E. Abuse by external heating, overcharge and short circuiting of commercial lithium-ion battery cells. *J. of The Electrochem. Soc.* **161**(10), A1611–A1617 (2014).
8. Larsson, F., Andersson, P. & Mellander, B.-E. Are electric vehicles safer than combustion engine vehicles? in *Systems perspectives on* Electromobility (eds. Sandén, B. & Wallgren, P.) 33–44 (Chalmers University of Technology, 2014).
9. Finegan, D. P. *et al*. In-operando high-speed tomography of lithium-ion batteries during thermal runaway. *Nat. Commun.* **6**, 6924 (2015).
10. Larsson, F., Andersson, P. & Mellander, B.-E. Lithium-ion battery aspects on fires in electrified vehicles on the basis of experimental abuse tests. *Batteries* **2**, 9 (2016).
11. Lopez, F. L., Jeevarajan, J. A. & Mukherjee, P. P. Experimental analysis of thermal runaway and propagation in lithium-ion battery modules. *J. of The Electrochem. Soc* **162**(9), A1905–A1915 (2015).
12. Lamb, J., Orendorff, C. J., Steele, L. A. M. & Spangler, S. W. Failure propagation in multi-cell lithium-ion batteries. *J. of Power Sources* **283**, 517–523 (2015).
13. Larsson, F., Anderson, J., Andersson, P. & Mellander, B.-E. Thermal modelling of cell-to-cell fire propagation and cascading thermal runaway failure effects for lithium-ion battery cells and modules using fire walls. *J. of The Electrochem. Soc.* **163**(14), A2854–A2865 (2016).
14. Lebedeva, N. P. & Boon-Brettz, L. Considerations on the chemical toxicity of contemporary Li-ion battery electrolytes and their components. *J. of The Electrochem. Soc.* **163**(6), A821–A830 (2016).
15. Sun, J. *et al*. Toxicity, a serious concern of thermal runaway from commercial Li-ion battery. *Nano Energy* **27**, 313–319 (2016).
16. Nedjalkov, A. *et al*. Toxic gas emissions from damaged lithium ion batteries–analysis and safety enhancement solution. *Batteries* **2**, 5 (2016).
17. Liu, K. *et al*. Electrospun core-shell microfiber separator with thermal-triggered flame-retardant properties for lithium-ion batteries. *Sci. Adv.* **3**, e1601978 (2017).
18. Park, Y.-U. *et al*. Tailoring a fluorophosphate as a novel 4 V cathode for lithium-ion batteries. *Scientific Reports* **2**, 704 (2012).
19. Ortiz, G. F. *et al*. Enhancing the energy density of safer Li-ion batteries by combining high-voltage lithium cobalt fluorophosphate cathodes and nanostructured titania anodes. *Scientific Reports* **6**, 20656 (2016).
20. Yang, H., Zhuang, G. V. & Ross Jr, P. Thermal stability of $LiPF_6$ salt and Li-ion battery electrolytes containing $LiPF_6$. *J. of Power Sources* **161**, 573–579 (2006).
21. Kawamura, T., Okada, S. & Yamaki, J.-i Decomposition reaction of $LiPF_6$-based electrolytes for lithium ion cells. *J. of Power Sources* **156**, 547–554 (2006).
22. Documentation for immediately dangerous to life or health concentrations (IDLHs) for hydrogen fluoride (as F). *The National Institute for Occupational Safety and Health (NOISH)* (1994).
23. Acute exposure guideline levels for selected airborne chemicals: volume 4, subcommittee on acute exposure guideline levels. ISBN: 0-309-53013-X. *Committee on Toxicology, National Research Council* (2004).
24. Middelman, A. Hygiensiska gränsvärden AFS 2015:7, Hygieniska gränsvärden. Arbetsmiljöverkets föreskrifter om hygieniska gränsvärden och allmänna råd om tillämpningen av föreskrifterna. ISBN 978-91-7930-628-1. ISSN 1650-3163. *Swedish Work Environment Authority* (2015).
25. Guéguen, A. *et al*. Decomposition of $LiPF_6$ in high energy lithium-ion batteries studied with online electrochemical mass spectrometry. *J. of The Electrochem. Soc.* **163**(6), A1095–A1100 (2016).

26. Chatelain, M. D. & Adams, T. E. Lithium ion gas sampling of vented cells. *Proceedings of the Power Sources Conference* **42**, 87–89 (2006).
27. Blum, A. F. & Long Jr, R. T. Hazard assessment of lithium ion battery energy storage systems. *Fire Protection Research Foundation* (2016).
28. Larsson, F., Andersson, P., Blomqvist, P., Lorén, A. & Mellander, B.-E. Characteristics of lithium-ion batteries during fire tests. *J. of Power Sources* **271**, 414–420 (2014).
29. Larsson, F., Andersson, P., Blomqvist, P. & Mellander, B.-E. Gas emissions from Lithium-ion battery cells undergoing abuse from external fire in *Conference proceedings of Fires in vehicles* (FIVE) 2016 (eds. Andersson, P. & Sundstrom, B.) 253–256 (SP Technical Research Institute of Sweden, 2016).
30. Ribière, P. *et al*. Investigation on the fire-induced hazards of Li-ion battery cells by fire calorimetry. *Energy Environ. Sci.* **5**, 5271–5280 (2012).
31. Lecocq, A. Scenario-based prediction of Li-ion batteries fire-induced toxicity. *J. of Power Sources* **316**, 197–206 (2016).
32. Lecocq, A., Bertana, M., Truchot, B. & Marlair, G. Comparison of the fire consequences of an electric vehicle and an internal combustion engine vehicle in *Conference proceedings of Fires in vehicles* (FIVE) 2012 (eds. Andersson, P. & Sundstrom, B.) 183–193 (SP Technical Research Institute of Sweden, 2012).
33. Ohsaki, T. *et al*. Overcharge reaction of lithium-ion batteries. *J. of Power Source* **146**, 97–100 (2005).
34. Abraham, D. P. *et al*. Diagnostic examination of thermally abused high-power lithium-ion cells. *J. of Power Sources* **161**, 648–657 (2006).
35. Roth, E. P. Abuse response of 18650 Li-ion cells with different cathodes using EC:EMC/$LiPF_6$ and EC:PC:DMC/$LiPF_6$ electrolytes. *ECS Transactions* **11**(19), 19–41 (2008).
36. Golubkov, A. W. *et al*. Thermal-runaway experiments on consumer Li-ion batteries with metal-oxide and olivin-type cathodes. *RSC Adv.* **4**, 3633–3642 (2014).
37. Golubkov, A. W. *et al*. Thermal runaway of commercial 18650 Li-ion batteries with LFP and NCA cathodes—impact of state of charge and overcharge. *RSC Adv.* **5**, 57171–57186 (2015).
38. Spinner, N. S. *et al*. Physical and chemical analysis of lithium-ion battery cell-to-cell failure events inside custom fire chamber. *J. of Power Sources* **279**, 713–721 (2015).
39. Fu, Y. *et al*. An experimental study on burning behaviors of 18650 lithium ion batteries using a cone calorimeter. *J. of Power Sources* **273**, 216–222 (2015).
40. Huang, P., Wang, Q., Li, K., Ping, P. & Sun, J. The combustion behavior of large scale lithium titanate battery. *Scientific Reports* **5**, 7788 (2015).
41. Ping, P. *et al*. Study of the fire behavior of high-energy lithium-ion batteries with full-scale burning test. *J. of Power Sources* **285**, 80–89 (2015).
42. Roth, E. P. & Orendorff, C. J. How electrolytes influence battery safety. *The Electrochem. Soc. Interface, summer* **2012**, 45–49 (2012).
43. Eshetu, G. G. *et al*. In-depth safety-focused analysis of solvents used in electrolytes for large scale lithium ion batteries. *Phys. Chem. Chem. Phys.* **15**, 9145–9155 (2013).
44. Lamb, J., Orendorff, C. J., Roth, E. P. & Langendorf, J. Studies on the thermal breakdown of common Li-ion battery electrolyte components. *J. of The Electrochem. Soc.* **162**(10), A2131–A2135 (2015).
45. Eshetu, G. G. *et al*. Fire behavior of carbonates-based electrolytes used in Li-ion rechargeable batteries with a focus on the role of the $LiPF_6$ and LiFSI salts. *J. of Power Sources* **269**, 804–811 (2014).
46. Andersson, P., Blomqvist, P., Lorén, A. & Larsson, F. Using Fourier transform infrared spectroscopy to determine toxic gases in fires with lithium-ion batteries. *Fire and Materials* **40**(8), 999–1015 (2016).
47. Lux, S. F. The mechanism of HF formation in $LiPF_6$ based organic carbonate electrolytes. *Electrochem. Comm.* **14**, 47–50 (2012).
48. Lux, S. F., Chevalier, J., Lucas, I. T. & Kostecki, R. HF formation in $LiPF_6$-based organic carbonate electrolytes. *ECS Electrochem. Lett.* **2**(12), A121–A123 (2013).
49. Wilken, S., Treskow, M., Scheers, S., Johansson, P. & Jacobsson, P. Initial stages of thermal decomposition of $LiPF_6$-based lithium ion battery electrolytes by detailed Raman and NMR spectroscopy. *RSC Adv.* **3**, 16359–16364 (2013).
50. Hammami, A., Raymond, N. & Armand, M. Runaway risk of forming toxic compounds. *Nat.* **424**, 635–636 (2013).
51. Campion, C. L. *et al*. Suppression of toxic compounds produced in the decomposition of lithium-ion battery electrolytes. *Electrochem. and Solid-State Lett.* **7**(7), A194–A197 (2004).
52. Liu, X. *et al*. Heat release during thermally-induced failure of a lithium ion battery: impact of cathode composition. *Fire Safety Journal* **85**, 10–22 (2016).
53. Lyon, R. E. & Walters, R. N. Energetics of lithium ion battery failure. *J. of hazardous materials* **318**, 164–172 (2016).
54. EN 13823:2010. Reaction to fire tests for building products–building products excluding floorings exposed to the thermal attack by a single burning item. *European Committee for Standardization* (2010).
55. EN 13501−1:2007 + A1:2009. Fire classification of construction products and building elements - part 1: classification using data from reaction to fire tests. *European Committee for Standardization* (2009).
56. ISO 19702:2006. Toxicity testing of fire effluents–guidance for analysis of gases and vapours in fire effluents using FTIR gas analysis. *International Organization for Standardization* (2006).
57. Andersson, P., Blomqvist, P., Lorén, A. & Larsson, F. Investigation of fire emissions from Li-ion batteries. *SP Technical Research Institute of Sweden*. SP Report 2013:5 (2013).
58. Hollas, J. M. Modern Spectroscopy, 3ed. (John Wiley & Sons, 1996).

Acknowledgements

The Swedish Energy Agency and its FFI-program, and Carl Tryggers Stiftelse för Vetenskaplig Forskning are acknowledged for their financial support. Several persons at RISE Research Institutes of Sweden and Chalmers University of Technology have been involved in this work and are gratefully acknowledged.

Author Contributions

F. Larsson planned the experiments, partially together with P. Andersson and B.-E. Mellander. P. Andersson made the initial data process of the SBI heat release data. P. Blomqvist planned and performed the FTIR and gas-washing bottles measurements and made the initial data processing. F. Larsson prepared the batteries and performed the measurement and data analyses of temperature, cell voltage and water mist, and did the post-measurements and final data processing. Water mist setup was planned and constructed by B.-E. Mellander and F. Larsson. All four authors were involved in the analyses of the data and wrote the paper.

Additional Information

Competing Interests: The authors declare that they have no competing interests.

Publisher's note: Springer Nature remains neutral with regard to jurisdictional claims in published maps and institutional affiliations.